TÜBİTAK

Turkish Journal of Chemistry

http://journals.tubitak.gov.tr/chem/

Research Article

Turk J Chem
(2021) 45: 634-646
© TÜBİTAK
doi:10.3906/kim-2010-5

Synthesis, characterization, and biological evaluation of new copper complexes of naphthyl pyrazole ligands

Melek HINIS[1], Kuldip SINGH[2], Demet ERDÖNMEZ[3], Ayfer MENTEŞ[1,*]

[1]Department of Chemistry, Faculty of Arts and Sciences, Aksaray University, Aksaray, Turkey
[2]Department of Chemistry, Leicester University, Leicester, England, UK
[3]Department of Biology, Faculty of Arts and Sciences, Aksaray University, Aksaray, Turkey

Received: 02.10.2020 • **Accepted/Published Online:** 08.02.2021 • **Final Version:** 30.06.2021

Abstract: Two naphthalene pyrazole ligands were synthesized using KOH/DMSO and Cu catalyst and characterized with FT-IR, ESI-MS, ^{1}H, and ^{13}C NMR spectroscopies. The crystal structures of 1-(2-methylnaphthalen-1-yl)-1H-pyrazole (MeNap-Pz) ligand have been determined with X-ray crystal structure analysis. Reaction of the ligands with $Cu(NO_3)_2x3.5H_2O$ gave two new complexes and characterized with magnetic susceptibility, molar conductance, FT-IR, LCMS-MS, ICP-OES, NMR, thermogravimetric analysis, and ESR spectra. The spectral data of the ligands are coordinated to the metal ion through the nitrogen atoms of the pyrazole ring. Consequently, it has been determined that $[Cu(MeNap\text{-}Pz)_2(NO_3)]NO_3.2H_2O$ complex showed square planar geometry and $[Cu(NapMe\text{-}Pz)_2(NO_3)_2].H_2O$ complex showed octahedral geometry. All compounds were screened for in vitro antibacterial activity and copper complexes have been shown to be effective on bacteria.

Key words: Naphthyl, pyrazole, copper, antimicrobial activity

1. Introduction

Pyrazole type ligands are very important in organometallic chemistry due to their wide usage area. Pyrazoles are aromatic ring organic compounds of the heterocyclic series with a 5-membered ring structure having three carbon and two nitrogen atoms [1–3]. Pyrazole derivatives exhibit many biological and pharmacological properties such as antibacterial, antiinflammatory, anticancer, antiviral, fungicidal, herbicidal, pesticide, and other biological activities [4–9]. In recent studies, it has been determined that naphthyl pyrazole ligands, which are pyrazole derivatives, and their metal complexes are also biologically active [10–12]. Pyrazole derivatives have also been used as ligands for formation of iridium complexes in organic light emitting diode (OLED) materials [13].

Due to the presence of two nucleophilic centers in the pyrazole ligands, the pyrazole nucleus being thermally and hydrolytically stable, the ability to coordinate in many ways and the pyrazole ligand to make hydrogen bonds, a wide variety of inorganic structures can be produced [14,15].

N-Aryl pyrazoles have been synthesized by reaction of 1,3-diketones with aryl hydrazines for many years. In accordance with the nature of the 1,3-diketones, undesirable isomers may be formed in such reactions [16]. In recent years, many methods that achieve heterocyclic N-arylation using catalytic Pd and Cu reactions have been reported [17]. Although the conditions in the N-arylation of the heterocyclic ligands using the Pd catalyst were mild [18], significant progress was made in the Cu-catalyzed N-arylation of pyrazoles due to both the high price of the Pd catalyst and the inadequate ligand concentration for the heterocyclic substrates [19,20]. For the direct arylation of pyrazole, bases such as KOH, KOt-Bu, or NaH are used in polar aprotic solvents such as DMSO, DMF [21–24].

Copper complexes of pyrazole are widely used. It is preferred in the synthesis of complexes because copper is easily available and insensitive to light or air, and it is the most economical way to form C–C bonds, which are increasingly important in both industrial and academic fields. Copper pyrazole complexes form thermally stable structures, and are used as effective catalysts in many reactions and biologically active structures are formed in the literature [25–27].

In this study, 1-(2-methylnaphthalen-1-yl)-lH-pyrazole (MeNap-Pz) and 1-(naphthalen-2-ylmethyl)-lH-pyrazole (NapMe-Pz) ligands were synthesized by the reaction of pyrazole with 1-bromo-2-methylnaphthalene and

* Correspondence: ayfermentes@yahoo.com

2-(bromomethyl) naphthalene in the KOH/DMSO system using Cu catalyst. Two novel copper(II) complexes with these ligands were obtained and characterized with FT-IR, NMR, and ESI-MS. The X-ray diffraction structures of the compound 1-(2-methylnaphthalen-1-yl)-l*H*-pyrazole (MeNap-Pz) were determined. The synthesized copper complexes were characterized with magnetic susceptibility, molar conductivity, FT-IR, NMR, LC MS-MS, ICP-OES, TGA, UV-Vis, and ESR spectra. All the synthesized compounds were evaluated for their antibacterial properties against various pathogenic bacterial strains (*Staphylococcus aureus*, *Pseudomonas aeruginosa*, *Klebsiella pneumoniae*, *and Bacillus cereus*) using the minimum inhibitory concentration method.

2. Materials and methods

All chemicals were purchased from Merck or Aldrich and were used without further purification. All solvents were dried and kept over molecular sieves prior to use.

The infrared spectra (4000–650 cm^{-1}) were recorded on a PerkinElmer Spectrum 100 FT-IR Spectrophotometer (PerkinElmer, Inc., Waltham, MA, USA) using the ATR technique. ^{1}H and ^{13}C-NMR spectra were measured on a Bruker DRX 400 MHz (Bruker, Corp., Billerica, MA, USA) or Agilent 600 MHz nuclear magnetic resonance instrument (Agilent Technologies, Inc., Santa Clara, CA, USA) ($CDCl_3$ and DMSO-d_6 as solvent).

Low-resolution electrospray ionization mass spectra (ESI-MS) were obtained on a micromass Quattro LC mass spectrometer (Waters, Corp., Milford, MA, USA) in acetonitrile or methanol as HPLC grade. Mass spectra LC-MS/MS were measured on a Thermo TSQ Quantum Access Max spectrometer (Thermo Scientific, Waltham, MA, USA). Copper contents of the complexes were obtained with PerkinElmer Optima 2100 DV inductively coupled plasma (ICP) optical emission spectrometry (OES).

Melting points were determined using Büchi B-540 brand melting point apparatus.

Thermogravimetric analyses (TGA) were performed under N_2 atmosphere at 1 atm with a heating rate of 10 °C/min on a PerkinElmer EXSTAR S11 7300 TG/DTA.

The ESR spectra were recorded with Jeol Jesfa-300 ESR X-band spectrometer using 9.5 GHz modulation.

UV-VIS spectra of the compounds were taken between 190 and 1000 nm using Genesys 10S UV-VIS spectrophotometer. Conductivities of solutions ($c = 1.0 \times 10^{-3}$ M in methanol) were measured in a 25 °C temperature with Table Top CD-2005 brand conductometer. Magnetic susceptibility of complexes was measured in a MK1 Sherwood Scientific magnetic susceptibility apparatus.

2.1. Synthesis of ligands

2.1.1. General comments

The materials used in the syntheses were all commercially available and were used without purification. All solvents were dried and kept over molecular sieves prior to use.

Although 1-(Naphthalen-2-ylmethyl)-1H-pyrazole (NapMe-Pz) ligand was synthesized by the cross-coupling reaction of aryl halides [28] and 1-(2-Methylnaphthalen-1-yl)-1H-pyrazole (MeNap-Pz) ligand was synthesized by microwave-assisted, cuprous oxide catalyzed coupling of aryl halides with pyrazole reaction [29] in previous studies, MeNap-Pz and NapMe-Pz ligands were synthesized using a modified method which includes the reaction of pyrazole with 1-bromo-2-methylnaphthalene or 2-(bromomethyl) naphthalene in the KOH/DMSO system using Cu catalyst for the synthesis of the ligands [30,31].

2.1.1.1. Synthesis of 1-(2-Methylnaphthalen-1-yl)-1*H*-pyrazole, (MeNap-Pz)

1-Bromo-2-methylnaphthalene (2.455 g, 10 mmol), pyrazole (1.090 g, 28 mmol), copper(I) oxide (0.150 g, 10 mmol), and KOH (1.15 g, 20 mmol) were stirred for 48 h in dried DMSO (20 mL) at 150 °C under a nitrogen atmosphere. The resulting black heterogeneous mixture was cooled to room temperature. Dichloromethane was added to the mixture and the mixture was filtered through silica to remove the pyrazole which did not enter the reaction. The solution was washed with water (4 × 25 mL) and dried with anhydrous $MgSO_4$. The solvent was removed on the rotary evaporator to obtain the crude product from the filtrate. TLC and ^{1}H NMR showed that the product was not pure; it was a mixture of MeNap-Pz and NapMe-Pz. The residue was purified with dichloromethane/petroleum ether (1:1) mixture by column chromatography from silica gel. Colorless NapMe-Pz crystals were obtained by recrystallization in CH_2Cl_2 and colorless MeNap-Pz crystals were obtained by recrystallization in petroleum ether. It was obtained as MeNap-Pz (Yield: 0.475 g, 22%; M.P. 62–74 °C) and NapMe-Pz (Yield: 0.277 g, 13%; M.P. 85–89 °C) (Scheme 1).

MeNap-Pz;

ES-MS (*m/z*): 208 [M], 192 [M-CH_3], 180 [M-HCN] (100%)

FT-IR (ATR, cm^{-1}): 3127-3047 $\upsilon(C\text{-}H)_{ar}$, 2922 $\upsilon(C\text{-}H)_{al}$, 1633 υ(C=N), 1599–1507 υ(C=C), 1370 υ(C-N), 1040 υ(N-N).

^{1}H NMR: (400 MHz, $CDCl_3$), δ (ppm): 7.87–7.83 (3H, m, H_{14}, H_{11}, H_9), 7.61 (1H, dd, H_3, J = 2.3 Hz), 7.46–7.39 (3H, m, H_{12}, H_{13}, H_5), 7.12 (1H, dd, H_8, J = 8.0 Hz), 6.55 (1H, t, H_4, J = 2.1 Hz), 2.21 (3H, s, CH_3).

^{13}C NMR ($CDCl_3$, 100.6 MHz), δ (ppm): 140.46 (C_3), 133.72 (C_6), 132.51 (2C; C_{10}, C_{15}), 131.55 (C_{11}), 129.12 (C_{14}), 128.31 (C_7), 127.64 (2C; C_5, C_8), 127.31 (C_{13}), 125.72 (C_{12}), 122.53 (C_9), 106.09 (C_4), 17.56 (CH_3).

2.1.1.2. Synthesis of 1-(Naphthalen-2-ylmethyl)-1*H*-pyrazole, (NapMe-Pz)

The 1-(Naphthalen-2-ylmethyl)-1*H*-pyrazole was synthesized and isolated with the same method as MeNap-Pz, using 2-(bromomethyl)naphthalene (0.982 g, 4 mmol) and pyrazole (0.436 g, 6.4 mmol) stirring for 48 h in dried DMSO (20 mL) at 150 °C under a nitrogen atmosphere. TLC and ^{1}H NMR results showed that the product was pure. It was obtained as colorless NapMe-Pz crystals (Yield: 0.453 g, 54 %; M.P. 85–89 °C) (Scheme 2). The analytical results of NapMe-Pz were determined to be the same as the compound in the first synthesized mixture in Scheme 1.

NapMe-Pz;

ES-MS (*m/z*): 207 [M^-], 180 [M-Pz] (100%)

FT-IR (ATR, cm^{-1}): 3130-3049 υ(C-H)$_{ar}$, 2970 υ(C-H)$_{al}$, 1737 υ(C=N), 1600–1509 υ(C=C), 1370 υ(C-N), 1047 υ(N-N).

^{1}H NMR: (400 MHz, $CDCl_3$), δ (ppm): 7.78 (3H, m, H_9, H_{11}, H_{14}), 7. 63 (1H, s, H_{16}), 7.56 (1H, dd, H_3, J = 1.5 Hz), 7.45 (2H, m, H_{12}, H_{13}), 7.37 (1H, d, H_5, J = 2.6 Hz), 7.30 (1H, dd, H_8, J = 8.2 Hz, J = 1.8 Hz), 6.27 (1H, t, H_4, J = 2.0 Hz), 5.44 (2H, s, H_6).

^{13}C NMR ($CDCl_3$, 100.6 MHz), δ (ppm): 139.57 (C_3), 134.06 (C_7), 133.31 (C_{15}), 132.97 (C_{10}), 129.25 (C_5), 128.68 (C_8), 127.91 (C_{11}), 127.69 (C_{14}), 126.69 (C_9), 126.36 (C_{16}), 126.21 (C_{13}), 125.39 (C_{12}), 106.03 (C_4), 56.09 (C_6).

2.2. Synthesis of complexes

2.2.1. Synthesis of [Cu(MeNap-Pz)$_2$(NO$_3$)]NO$_3$.2H$_2$O complex

1 mmol (0.208 g) of MeNap-Pz dissolved in acetonitrile (8 mL) was added to a solution of $Cu(NO_3)_2x3.5H_2O$ (1 mmol, 0.250 g) in acetonitrile (20 mL). The mixture was heated to reflux for 4 h and its color turned to green. TLC showed that

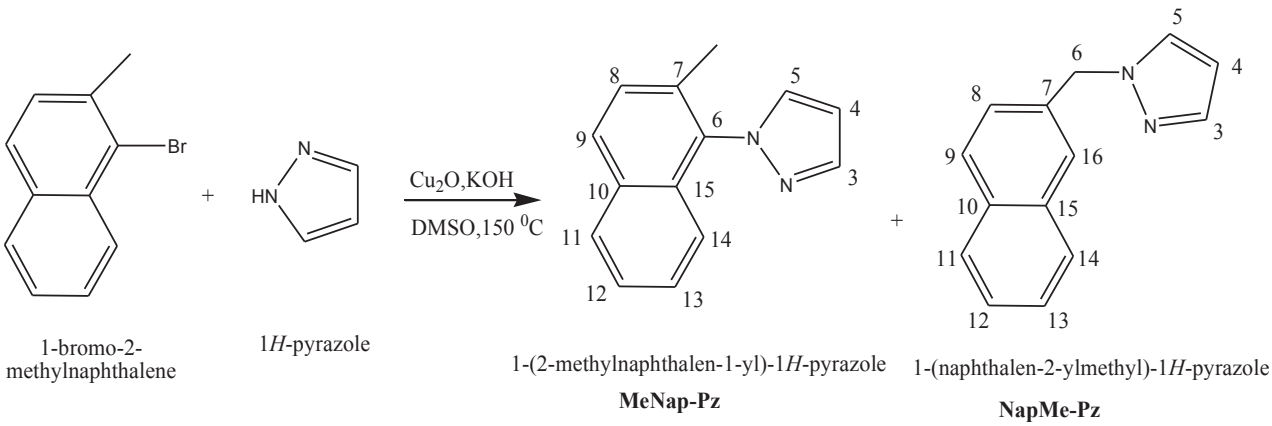

Scheme 1. MeNap-Pz and NapMe-Pz ligands synthesis scheme.

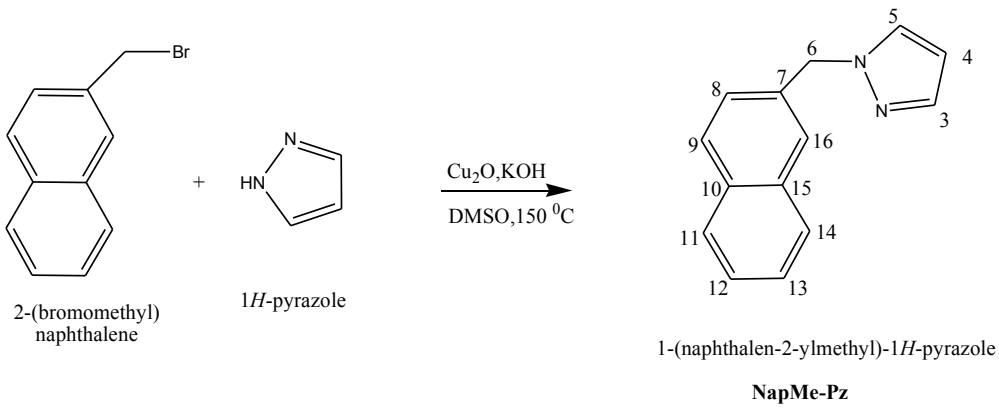

Scheme 2. NapMe-Pz synthesis scheme.

the complex was formed. After evaporation, the green solid was filtered off, and washed with diethyl ether and dried at room temperature (DTG_{mak}: 220 °C, M/L: 1/1, Yield: 0.333 g, 52 %). Purity of the complex was checked by TLC (Scheme 3).

LC-MS/MS (*m/z)*: 541 $[ML_2NO_3]^+$, ICP-OES wt% of Cu, found (Calc.%): 11.90 (10.21).

Λ_M: 129 Ω^{-1} cm^2 mol^{-1}.

FT-IR (ATR, cm^{-1}): 3545 υ(O-H; H_2O), 3128–3054 υ(C-H)$_{ar}$, 2916 υ(C-H)$_{al}$, 1635 υ(C=N), 1601–1577 υ(C=C), 1373 υ(C-N), 1062 υ(N-N), 1480, 1277, 1011 υ(N-O, NO_3).

^{1}H-NMR (600 MHz, DMSO-d_6), δ (ppm): 7.9–6.9 (br, H-Ar), 6.5 (H_4-Pz), 2.0 (H-CH_3).

^{13}C-NMR (150 MHz, DMSO- d_6), δ (ppm): 133.5–122.4 (C-Ar), 140.7 (C_3-Pz), 135.4 (C_5-Pz), 106.9 (C_4-Pz), 17.5 (CH_3).

2.2.2. Synthesis of $[Cu(NapMe\text{-}Pz)_2(NO_3)_2].H_2O$ complex

0.2 mmol (0.04 g) of NapMe-Pz dissolved in acetonitrile (5 mL) was added to a solution of $Cu(NO_3)_2x3.5H_2O$ (0.06 mmol, 0.016 g) in acetonitrile (4 mL). The mixture was heated to reflux for 5 h and its color turned from brown to green. TLC showed that the complex was formed. After evaporation, the green jelly-like substance was obtained. The complex was washed with ethanol and dried at room temperature (DTG_{mak}: 242 °C, Yield: 0.249 g, 40 %). Purity of the complex was checked with TLC (Scheme 4).

LC-MS/MS (*m/z)*: 639 $[ML_2NO_3]^+$,, ICP-OES wt % of Cu, found (Calc.%): 9.34 (9.92).

Λ_M: 13 Ω^{-1} cm^2 mol^{-1}.

FT-IR (ATR, cm^{-1}): 3409 υ(O-H, H_2O), 3132–3050 υ(C-H)$_{ar,}$, 2972–2947 υ(C-H)$_{al}$, 1633 υ(C=N), 1602 υ(C=C), 1396 υ(C-N), 1049 υ(N-N), 1483, 1275, 1010 υ(N-O, NO_3).

2.3. X-ray crystal structure determination

Colorless crystals of MeNap-Pz for X-Ray diffraction experiments were obtained with recrystallization in petroleum ether. Details of the structure determinations of MeNap-Pz are summarized in Table 1. Data were collected on a Bruker Apex 2000 CCD diffractometer using graphite-monochromated Mo KR radiation, λ = 0.7107 Å at 150 K. The data were corrected for Lorentz and polarization effects, and empirical absorption corrections (SADABS) [32] were applied in all cases. The structures were solved using Patterson methods and refined with full-matrix least-squares on F^2 using the program SHELXTL [33]. All hydrogen atoms bonded to carbon were included in calculated positions (C-H = 0.96 Å)

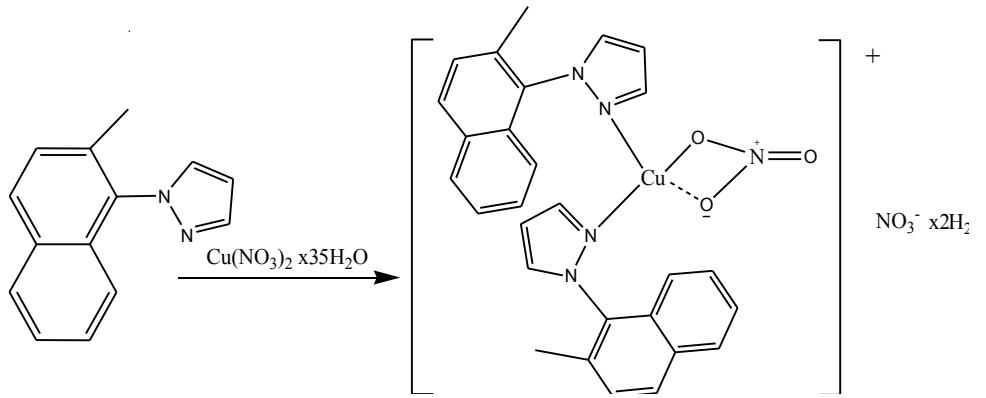

Scheme 3. The synthesis scheme of the [Cu(MeNap-Pz)2(NO3)]NO3.2H2O complex.

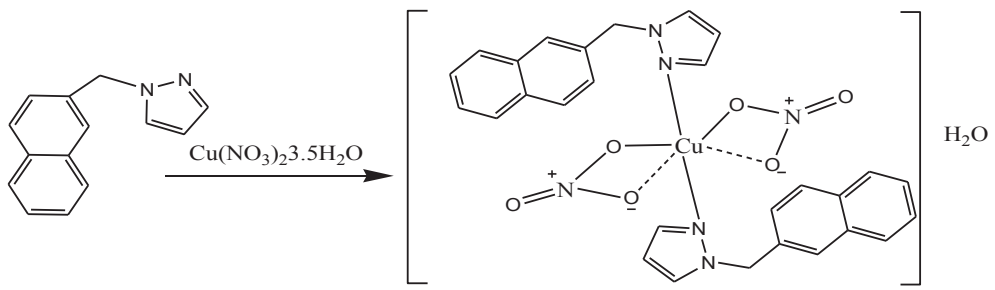

Scheme 4. The synthesis scheme of the $[Cu(NapMe\text{-}Pz)_2(NO_3)_2].H_2O$ complex.

Table 1. Crystal data and structure refinement for MeNap-Pz

Empirical formula	$C_{14}H_{12}N_2$
Formula weight	208.26
Temperature, K	150(2)
Wavelength, Å	0.71073
Crystal system	Triclinic
Space group	P-1
a, Å	7.589(2)
b, Å	8.060(2)
c, Å	9.040(3)
α, deg	77.908(5)
β, deg	85.503(5)
γ, deg	84.705(5)
Volume, $Å^3$	537.4(3)
Z	2
Density (calculated), Mg/ m^3	1.287
Absorption coefficient, mm^{-1}	0.077
F(000)	220
Crystal size, mm^3	0.34 x 0.32 x 0.24
Theta range for data collection	2.31 to 24.97°.
Index ranges	-9<=h<=9, -9<=k<=9, -10<=l<=10
Reflections collected	3886
Independent reflections	1877 [R(int) = 0.0380]
Completeness to theta = 24.97°	99.0 %
Absorption correction	Empirical
Max. and min. transmission	0.969 and 0.517
Refinement method	Full-matrix least-squares on F^2
Data / restraints / parameters	1877 / 0 / 146
Goodness-of-fit on F^2	1.087
Final R indices [I>2sigma(I)]	R1 = 0.0588, wR2 = 0.1533
R indices (all data)	R1 = 0.0729, wR2 = 0.1618
Largest diff. peak and hole	0.223 and -0.208 e.$Å^{-3}$

using a riding model. Figures were drawn using the program ORTEP [34]. All nonhydrogen atoms were refined with anisotropic displacement parameters without positional restraints.

Atomic coordinates, bond lengths and angles, and thermal parameters have been deposited at the Cambridge Crystallographic Data Centre, CCDC Nos. 1944106.

2.4. Antibacterial activity

All the synthesized ligands and their corresponding Cu(II) complexes were screened in vitro for their biological activity by using two gram-positive bacteria, namely *Staphylococcus aureus* ATCC 29213, *Bacillus cereus* ATCC 10876 and two gram-negative bacteria, namely *Pseudomonas aeruginosa* ATCC 27853 and *Klebsiella pneumoniae* ATCC 700603, which caused widespread hospital infections and severe antibiotic resistance. Well diffusion method was used in antimicrobial activity trials. After 100 µL of previously produced microorganism culture was adjusted according to McFarland 0.5 (1.5×10^8 CFU/mL) turbidity, it was inoculated on the surface of Mueller-Hinton agar by sterile swab spreading. Under sterile conditions, 5 mm diameter wells were dug in the agar media using a cork borer. Ligands and copper complexes were

prepared at a concentration of 90 mg/mL, 20 µL was added to the individual wells and the culture was incubated for 24 h at 37 °C. Standard antibacterial drug (gentamycine) was screened under similar conditions for comparison. Activity was determined at the end of 24 h by measuring the diameter of the zone showing complete inhibition (mm) and the experiments were performed in 3 replications [35,36].

2.5. Minimum inhibitory concentration (MIC)

It was determined using the microdilution method according to procedures developed by the National Committee of Clinical Laboratory Standards [37]. The minimum inhibitory concentration was determined by assaying at 90 mg/mL, 45 mg/mL, 22.5 mg/mL, 11.25 mg/mL, and 5.625 mg/mL concentrations along with standards at the same concentrations. The lowest compound concentration inhibiting visible bacterial growth is reported as MIC. The experiment was repeated 3 times.

3. Result and discussion

The reaction of pyrazole with 1-bromo-2-methylnaphthalene gave a mixture of two ligands (MeNap-Pz and NapMe-Pz). Because bromine atom that was bonded to seconder carbon of naphthalene led to halogen migration to methyl group, NapMe-Pz ligand was produced as a by-product. Therefore, it was decided to perform the reaction of pyrazole with 2-(bromomethyl)naphthalene to obtain NapMe-Pz. Analytical results verified the proposed formulas for the MeNap-Pz and NapMe-Pz compounds. NMR, FT-IR, and mass spectra results of these ligands were confirmed by comparison with the structures of synthesized compound previously [28,29]. Copper complexes of the MeNap-Pz and NapMe-Pz ligands were synthesized for the first time and characterized with NMR, FT-IR, mass spectra, UV-Vis, and ESR. Although MeNap-Pz and NapMe-Pz ligands were soluble in organic polar solvents, they were sparingly soluble in EtOH. Complexes were soluble in organic solvents such as EtOH, MeOH, acetonitrile, and acetone, while they were insoluble in water and nonpolar organic solvents such as diethyl ether, hexane, and petroleum ether. Although NapMe-Pz ligand had poor solubility in EtOH, complex of $[Cu(NapMe\text{-}Pz)_2(NO_3)_2].H_2O$ was soluble in EtOH.

The infrared data of pyrazole ligands and their Cu complexes (Figures S1–S4) are summarized in Table 2. The IR spectra of pyrazole ligands show weak absorption bands in the range of 3130–3047 cm^{-1} indicating the presence of the aromatic C–H stretching vibrations. Absorption bands at 2970–2922 cm^{-1} should be assigned to the stretching vibrations of the C–H (-CH_3, -CH_2). Another characteristic pyrazole bands in the range of 1737–1633 cm^{-1} (C=N), 1600–1500 cm^{-1} (C=C), 1370 cm^{-1} (C-N), and 1047–1040 cm^{-1} (N-N) are attributed to the aromatic skeleton stretching vibration of the pyrazolyl and naphthyl rings [30,38]. The IR spectra data of the complexes $[Cu(MeNap\text{-}Pz)_2(NO_3)]NO_3.2H_2O$ and $[Cu(NapMe\text{-}Pz)_2(NO_3)_2].H_2O$ showed lattice water absorbs at 3545–3409 cm^{-1} [39] and showed stretching vibrations of aromatic C–H and aliphatic C–H (-CH_3, -CH_2) in the range of 3128–3050 cm^{-1} and 2972–2916 cm^{-1}, respectively. The shift of the C=N, C=C, C-N, and N-N of the pyrazole and naphthaline rings bands frequencies compared to that of the free ligands bonds showed the interaction between Cu(II) and pyrazole ligands [30]. The characteristic bands of NO_3^- anion are shown at 1483–1480 cm^{-1} for asymmetric stretching vibrations (υ_5), 1277–1275 cm^{-1} for symmetric stretching vibrations (υ_1) and 1011–1010 cm^{-1} for (N=O) stretching vibrations (υ_2). The coordination modes of the nitrate ions are important in clarifying the geometric structures of the synthesized copper nitrate complexes. The nitrate ion can be bonded to the

Table 2. The important infrared frequencies (in cm^{-1}) of naphthyl-pyrazole ligands and Cu(II) complexes.

	MeNap-Pz	NapMe-Pz	$[Cu(MeNap\text{-}Pz)_2(NO_3)]NO_3.2H_2O$	$[Cu(NapMe\text{-}Pz)_2(NO_3)_2].H_2O$
υ(O-H)			3545	3409
$\upsilon(C\text{-}H)_{ar}$	3127–3047	3130–3049	3128–3054	3132–3050
$\upsilon(C\text{-}H)_{al}$	2922	2970	2916	2972–2947
υ(C=N)	1633	1737	1635	1633
υ(C=C)	1599–1507	1600–1509	1601–1577	1602
υ(C-N)	1370	1370	1373	1396
υ(N-N)	1040	1047	1062	1049
$\upsilon(N\text{-}O, NO_3)$			1480 (υ_5) 1277 (υ_1) 1011 (υ_2)	1483 (υ_5) 1275 (υ_1) 1010 (υ_2)

metal in different fashions, such as monodentate, bidentate, or chelated bridges in the copper(II) nitrate complexes. Large splitting of stretching vibrations of N–O bonds in a NO_3^- ion (υ_5-υ_1>160) confirms the presence of bidentate nitrate ions of complexes [39–41]. The presence of coordinated water molecules in the complexes is indicated by a broad band in the region 3545–3409 cm^{-1} [42]. IR spectral data results indicate that naphthyl-pyrazole ligands and their Cu(II) complexes were obtained.

^1H and ^{13}C NMR spectra of ligands (Figures S5–S8) were recorded in $CDCl_3$. In ^1H NMR, MeNap-Pz and NapMe-Pz ligands showed the aromatic protons at δ = 7.1–7.8 ppm and a typical proton signal (H_4) at δ = 6.5 ppm, (CH_3) at δ = 2.2 ppm for MeNap-Pz and (H_4) at δ = 6.2 ppm, (CH_2) at δ = 5.4 ppm for NapMe-Pz. In ^{13}C-NMR ($CDCl_3$) spectra of ligands showed the aromatic carbons for naphthalene at δ = 134–122.5 ppm. Overlapping occurrences are observed because some of the aromatic ring carbons are symmetrical. The signals were observed at δ = 140.4 ppm and δ = 139.5 ppm for pyrazole (C_3) and (C_5) carbons and specific signal for pyrazole at δ = 106 ppm for (C_4) carbon for both of ligands. The signals of CH_2 carbon of NapMe-Pz and CH_3 carbon of MeNap-Pz were observed at δ = 56 ppm and δ = 17.5 ppm, respectively. NMR data confirms the proposed structure of the ligands [30,43,44]. NMR spectra of both complexes were measured, but the spectrum of $[Cu(NapMe\text{-}Pz)_2(NO_3)_2].H_2O$ complex was broad due to the paramagnetic property of copper and the signals could not be observed clearly. Although the spectrum of $[Cu(MeNap\text{-}Pz)_2(NO_3)]NO_3.H_2O$ complex was observed considerably broad compared to spectrum of ligand, its structure was fully clarified (Figures S9 and S10). Aromatic ring protons (C-H) was observed at δ = 9.9–7.9 ppm and pyrazole protons (H_4) at δ = 6.5 ppm and CH_3 protons at δ = 2.2 ppm in the ^1H NMR (DMSO-d_6) spectra of complex. Aromatic carbons were observed at δ = 134–122.5 ppm for naphthaline and pyrazole carbons at δ = 140.7 ppm (C_3) and δ = 135.4 ppm (C_5) in the ^{13}C NMR (DMSO-d_6) spectrum of complex. Chemical shift of the pyrazole carbon (C_5) moved to high frequency on the complex. In the HETCOR-NMR spectrum of the $[Cu(MeNap\text{-}Pz)_2(NO_3)]NO_3.2H_2O$ complex (Figure S11), it is seen that the numbers and signals of the hydrogen atoms and the carbon atoms in the aromatic ring are matched. Moreover, the pyrazole C_4 carbon at 106.9 ppm matched the H_4 proton at 6.5 ppm and the CH_3 group carbon at 17.5 ppm matched proton signals at 2.0 ppm.

NMR spectra were consistent with the signal values of the ligand and a slight shift was observed especially in ^1H-NMR values due to the binding to the metal. It was also confirmed by HETCOR-NMR that the number of hydrogen atoms attached to the aromatic ring was the same as the ligand, so the ligand was not orthomethalated with copper over the carbon in the aromatic ring.

MeNap-Pz molecular structure with the atom-numbering scheme is shown in Figure 1, and selected bond lengths and angles are given in Table 3. In the structure of the ligand, all carbon atoms of the naphthyl and pyrazole ring form a good plane, and the average of C–C distances and C–C–C angles from the ring are consistent with those reported in the literature [45]. The naphthyl and pyrazole rings are almost orientated perpendicular to each other at an angle of 80.62(13)°.

The TG and DTG curves for the complexes are shown in Figures S12 and S13. Table 4 lists the results of the thermal studies of these complexes. The decomposition of the complex $[Cu(MeNap\text{-}Pz)_2(NO_3)]NO_3.2H_2O$ in CuO occurs in three steps. In the first stage (99.4 °C), loss of two molecules water 5.91% (Calcd. 5.6%) of the total weight is observed. In the next stage of decomposition (220 °C), there is loss of 66.15% (Calcd. 65%) of the total weight attributed to the elimination of MeNap-Pz ligand [30]. The complex then showed a third weight loss in the range of 300–776 °C, a loss of 27.23% (Calcd. 29.37%), which corresponds to loss of NO_3^- and residue of CuO [46]. The TG–DTG curves for complex $Cu(NapMe\text{-}Pz)_2(NO_3)_2].H_2O$ (Figure S12) indicated that in the first stage (132.8 °C), there is loss of a water molecule 2.2% (Calcd. 2.89%) of the total weight. In the second stage of decomposition (242.4 °C), there is loss of 63.69 (calcd. 66.87%) of total weight attributed to the elimination of NapMe-Pz ligand [30]. In the third stage, the loss of NO_3^- anions 22.59% (calcd. 19.93%) is in the range of 300–600 °C [46]. The final decomposition residue was CuO 11.25% (calcd. 10.21%) over the range of 600 °C.

Molecular ion peak of MeNap-Pz was determined as 208 in Figure S14. The peaks obtained by removal of $–CH_3$ and HCN from pyrazole of the ligand were observed at 192 and 180 [M-HCN] (100%), respectively. In Figure S15, NapMe-Pz ligand molecular ion peak is [M-] 207 and the peak obtained by removal of pyrazole from the ligand was observed at 141 [M-Pz] (100%). Pyrazole bonded to methylene bridge ($-CH_2-$) was removed easily than that bonded to aromatic naphtyl group. The LC-MS/MS spectra of these complexes (Figures S16 and S17) are summarized in Table 5. Molecular ion peaks for $[Cu(NapMe\text{-}Pz)_2(NO_3)_2].H_2O$ (F.W.: 622 g/mol): $[Cu(NapMe\text{-}Pz)_2(NO_3)]^+$, 538, $[Cu(NapMe\text{-}Pz)_2]^{+2}$ ·479, and peak of NapMe-Pz (M.W.: 208 g/mol) ligand was observed at 209. Molecular ion peaks for $[Cu(MeNap\text{-}Pz)_2(NO_3)]NO_3.2H_2O$ (F.W.: 640 g/mol): $[Cu(MeNap\text{-}Pz)_2(NO_3)]^+$ (F.W.: 542 g/mol), $[Cu(MeNap\text{-}Pz)_2]^{+2}$ (F.W.: 480 g/mol), [MeNap-Pz] (M..W: 208 g/mol) were seen at 541, 481, 209, respectively.

Analytical and spectroscopic data of the synthesized complexes are given in Table 5. Complexes conductivity measured in 1×10^{-3} M methanol. The reported values for 1:1 and 1:2 electrolytes in methanol are 80–115 and 160–220 $\Omega^{-1}cm^2mol^{-1}$

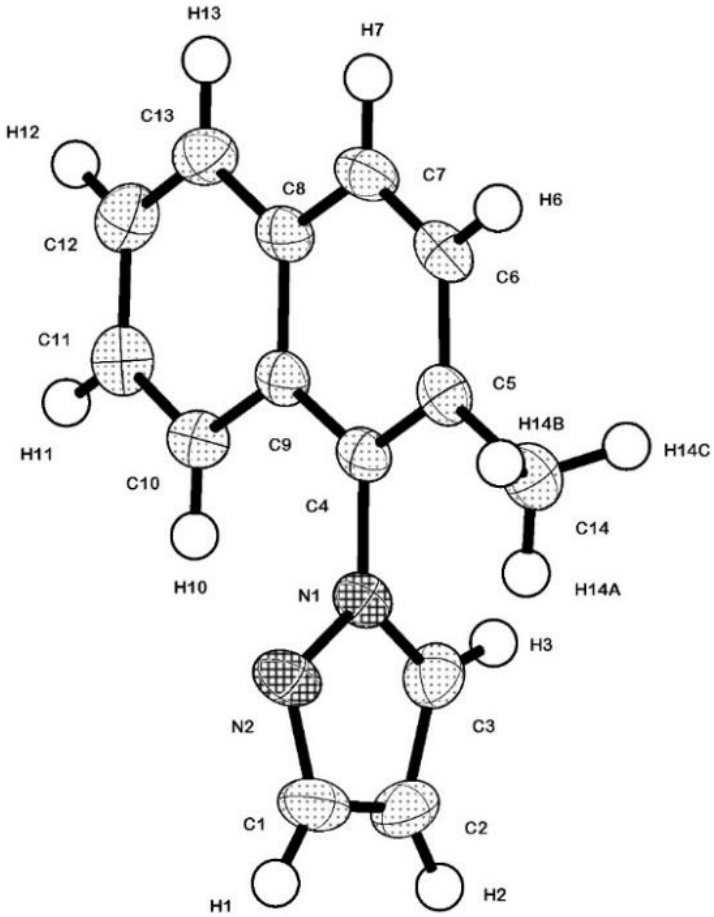

Figure 1. View of MeNap-Pz with the atom-labeling scheme and 50% probability displacement ellipsoids.

Table 3. Bond lengths [Å] and angles [°] for MeNap-Pz.

Bond lengths	(Å)	Angles	(°)
N(1)-C(3)	1.342(3)	C(3)-N(1)-N(2)	111.88(18)
N(1)-N(2)	1.362(2)	C(1)-N(2)-N(1)	103.77(19)
N(1)-C(4)	1.435(3)	C(3)-N(1)-C(4)	127.22(18)
N(2)-C(1)	1.332(3)	N(2)-C(1)-C(2)	112.2(2)
C(1)-C(2)	1.388(4)	C(3)-C(2)-C(1)	104.8(2)
C(2)-C(3)	1.363(3)	N(1)-C(3)-C(2)	107.4(2)
C(5)-C(14)	1.505(3)	C(6)-C(5)-C(14)	119.71(19)

[47]. Complexes conductivity in methanol ranged between 13 and 129, which is consistent with $[Cu(NapMe\text{-}Pz)_2(NO_3)_2]$. H_2O is nonionic and $[Cu(MeNap\text{-}Pz)_2(NO_3)](NO_3).2H_2O$ is electrolyte 1:1.

The experimental magnetic moment of the complex was found to be 1.75 and 2.27 B.M. The results showed that both complexes are paramagnetic and Cu is coordinated to ligands as mononuclear. The value of $[Cu(NapMe\text{-}Pz)_2(NO_3)_2].H_2O$ complex is in accordance with their distorted octahedral configurations [48]. According to the ICP-OES results, wt % Cu of the complexes were found and compared well with their theoretical values.

The electronic spectra of ligands and their copper(II) complexes were recorded and spectral data are given in Table S1 and Figures S18 and S19. Compared with the π–π^*transition of the ligands with complexes, the slight movement of the

Table 4. Thermal analysis data for the complexes.

	$[Cu(MeNap\text{-}Pz)_2(NO_3)]NO_3.2H_2O$ F.W.: 640 g/mol	$[Cu(NapMe\text{-}Pz)_2(NO_3)_2].H_2O$ F.W.: 622.09 g/mol
ΔT (°C)	50–100 100–776 776–800	100–200 100–300 300–600
Δm(Exp) (%)	5.91 66.15 27.23	2.2 63.69 22.59 11.25
Δm(Calcd.) (%)	5.63 65 29.37	2.89 66.87 19.93 10.31
Decomp. Steps	CuO	CuO
$DTG_{(peak)}$ (°C)	99.4 220 776	132.8 242.4

Table 5. Physical and analytical data for the complexes.

Complex	Color	Yield %	Mass LC-MS/MS (Calc.)	Conductivity $\Omega^{-1}cm^2mol^{-1}$	Magnetic Susceptibility BM	% Cu Exp. (Calc.)
$[Cu(MeNap\text{-}Pz)_2(NO_3)](NO_3).2H_2O$	Green	52	633 (640)	129	1.75	11.90 (10.21)
$[Cu(NapMe\text{-}Pz)_2(NO_3)_2].H_2O$	Green	40	623 (622.9)	13	2.27	9.34 (9.92)

absorption band of the complexes indicates the charge transfer from ligand to metal or metal to ligand [49]. The presence of strong absorption bands at 225 and 223 nm in the complexes indicates that there are ligand-centered bands. In the complexes, additional bands caused by δ–δ* transitions of Cu^{2+} were not seen. The reason why additional bands do not clearly appear in the complexes is thought to be that the π–π* transitions of the ligands overlap with other transitions by giving strong absorption bands.

The ESR spectra of copper(II) complexes in powder samples (Figures S20 and S21 and Table S2) were recorded at room temperature.

The ESR spectrum of $[Cu(MeNap\text{-}Pz)_2(NO_3)]NO_3.2H_2O$ complex shows g_{11} (2.21) > $g_\perp$ (2.05) value is characteristic of an axially elongated square-planar geometry. If the copper content in the compound is high, the hyperfine line from either ^{63}Cu or ^{65}Cu cannot be observed. The ESR results are $g_{11} > g_\perp > 2.00$ and this is a characteristic feature of $dx^2\text{-}y^2$ ground state [50,51]. Considering the ESR spectra, square planar geometry for this complex was suggested and copper(II) ion in this this complex in a tetragonal field (D4h) symmetry [52]. ESR results give the geometric parameter, G which is defined (Eq. 1) as

$$G = g_\parallel - 2.0023/g_\perp - 2.0023 \quad \text{(Eq.1)}$$

G value of the complex 3.9 < 4, suggesting unit cell contains magnetically equivalent ions and ligands are strong field in character [51,52]. According to our results, the G value is less than 4, which means that significant exchange coupling is present [50]. The ESR signals of $[Cu(NapMe\text{-}Pz)_2(NO_3)_2].H_2O$ complex shows well-resolved four line hyperfine splits because copper has a nuclear spin of (I = 3/2) which couples with the electron spin [42]. The observed spectral parameter of complex A_{11} (157) > $A_\perp$ (99) and g_{11} (2.35) > $g_\perp$ (2.03) indicates that the complex exerts an octahedral geometry [53].

The ESR results are $g_{11} > g_{\perp} > 2.00$ and this is indicative of a d_{x2-y2} ground state. G value of the complex 10.6 > 4, indicating that the exchange coupling effects are not operative in the present system. The reason is that large volume of ligands can be considered to reduce the exchange interactions between Cu(II) centers [54]. If G is greater than 4, local tetragonal axes are aligned parallel or only slightly misaligned [50].

The antibacterial results are presented in Tables 6 and 7 and Figure 2. Gentamycine was used as reference for antibacterial studies. In vitro antibacterial activity data reveals that the antibacterial activity of copper(II) complexes is higher than that of the ligands. As can be seen from Table 6, the greatest effect occurred on gram-positive bacteria *S. aureus* and *B. cereus*. All compounds display least activity against gram-negative bacteria *P. aeruginosa* and *K. pneumoniae*. While the MeNap-Pz ligand shows slight activity against *S. aureus*, the NapMe-Pz ligand is inactive towards all bacteria. While $[Cu(NapMe\text{-}Pz)_2(NO_3)_2].H_2O$ complex shows moderate activity against gram-positive bacteria, $[Cu(MeNap\text{-}Pz)_2(NO_3)]NO_3.2H_2O$ complex shows significant activity against all bacteria especially the gram-positive bacteria.

The minimum inhibitory concentration (MIC) data of the compounds are represented in Table 7. Depending on the concentration, the suppression of bacterial growth increases, but the effectiveness has not been observed because some compounds' concentration remains low. It can be said that NapMe-Pz and MeNap-Pz ligands have no activity on bacteria. Only MeNap-Pz ligand is active (MIC: 45 mg/mL) against *S. aureus* bacteria. Looking at these results of the complexes, while $[Cu(MeNap\text{-}Pz)_2(NO_3)]NO_3.2H_2O$ complex is highly active (MIC: 11.25 mg/mL) against *S. aureus*, it is inactive against *B. cereus* bacteria. On the other hand, it is active (MIC: 90 mg/mL) against *P. aeruginosa* and *K. pneumoniae* bacteria with the same concentration. While $[Cu(NapMe\text{-}Pz)_2(NO_3)_2].H_2O$ complex is very much active (MIC: 5.625 mg/mL) against *S. aureus*, it is inactive against *P. aeruginosa* and *K. pneumoniae* bacteria.

4. Conclusion

Pyrazole derivative ligands, 1-(2-methylnaphthalen-1-yl)-lH-pyrazole (MeNap-Pz) and 1-(naphthalen-2-ylmethyl)-lH-pyrazole (NapMe-Pz), were synthesized in the KOH/DMSO system using Cu catalyst and characterized with FT-IR, NMR,

Table 6. In vitro antimicrobial activity by using the agar diffusion method of tested the compounds.

Microorganism inhibition zone diameter mm (Relative inhibition %)				
Compound	Gram+ bacteria		Gram– bacteria	
	Staphylococcus aureus	*Bacillus cereus*	*Klebsiella pneumoniae*	*Pseudomonas aeruginosa*
NapMe-Pz	0(0)	0(0)	0(0)	0(0)
MeNap-Pz	6(28)	0(0)	0(0)	0(0)
$[Cu(NapMe\text{-}Pz)_2(NO_3)_2].H_2O$	12(57)	10(67)	0(0)	0(0)
$[Cu(MeNap\text{-}Pz)_2(NO_3)]NO_3.2H_2O$	14(67)	13(87)	6(37)	6(43)
Gentamycine (10 μg)	21(100)	15(100)	16(100)	14(100)

Table 7. Minimum inhibition concentration of compounds.

Compound	*Staphylococcus aureus* ATCC 29213		*Pseudomonas aeruginosa* ATCC 27853		*Klebsiella pneumoniae* ATCC 700603		*Bacillus cereus* ATCC 10876	
	MIC	MBC	MIC	MBC	MIC	MBC	MIC	MBC
NapMe-Pz	x	x	x	x	x	x	x	x
MeNap-Pz	1/2	1/2	x	x	x	x	x	x
$[Cu(NapMe\text{-}Pz)_2(NO_3)_2].H_2O$	1/16	1/16	x	x	x	x	1/4	1/4
$[Cu(MeNap\text{-}Pz)_2(NO_3)]NO_3.2H_2O$	1/8	1/8	1	1	1	1	x	x

MIC: Minimum inhibition concentration; MBC: Minimum bactericidal concentration; x = no effect concentration
*1 = 90 mg/mL, 1/2 = 45 mg/mL, 1/4= 22.5 mg/mL, 1/8 =11.25 mg/mL, 1/16 = 5.625 mg/mL.

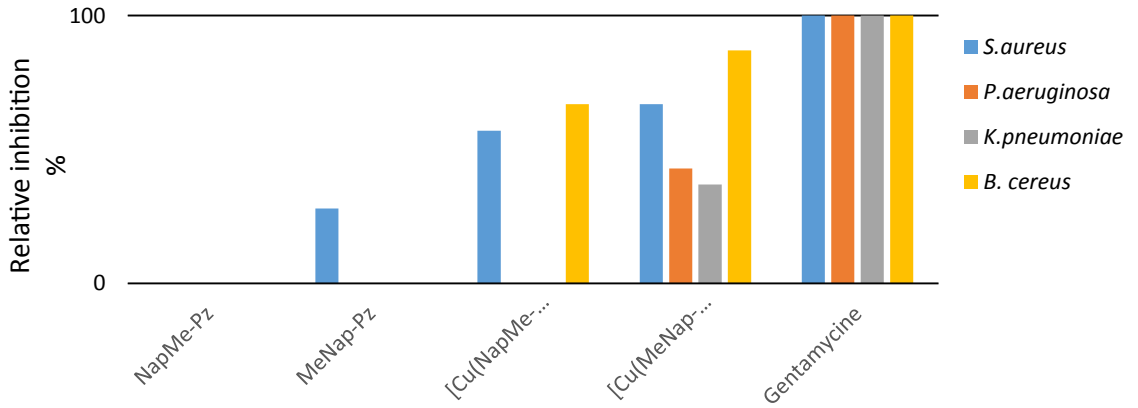

Figure 2. Antibacterial activity of synthesized ligands and complexes.

and ESI-MS. The X-ray diffraction structures of the compound MeNap-Pz were determined for the first time. $[Cu(NapMe\text{-}Pz)_2(NO_3)_2].H_2O$ and $[Cu(MeNap\text{-}Pz)_2(NO_3)](NO_3).2H_2O$ complexes were synthesized and characterized using magnetic susceptibility, molar conductivity, FT-IR, NMR, LC MS-MS, ICP-OES, TGA, and ESR spectra. $[Cu(NapMe\text{-}Pz)_2(NO_3)_2].H_2O$ complex is nonionic and $[Cu(MeNap\text{-}Pz)_2(NO_3)](NO_3).2H_2O$ complex is electrolyte 1:1 as a result of conductivity in methanol 13 and 129 $\Omega^{-1}cm^2mol^{-1}$, respectively. The ESR spectra of $[Cu(MeNap\text{-}Pz)_2(NO_3)]NO_3.2H_2O$ complex shows an axially elongated square-planar geometry and $[Cu(NapMe\text{-}Pz)_2(NO_3)_2].H_2O$ complex shows an octahedral geometry.

The synthesized compounds were tested with antibacterial screening. The new Cu(II) complexes show better antibacterial activity than ligands. Although $[Cu(MeNap\text{-}Pz)_2(NO_3)](NO_3).2H_2O$ complex has the highest recorded inhibition zones for antibacterial activities, it has low MIC values. $[Cu(NapMe\text{-}Pz)_2(NO_3)_2].H_2O$ complex has moderate recorded inhibition zones and strong MIC values for gram-positive bacteria, namely *S. aureus*. Therefore, the new Cu(II) complexes may be effective for the further development of biologically active agents.

Acknowledgments
The author is grateful to Prof David L. Davies and Leicester University for the use of X-ray diffractometer. The authors thank Aksaray University Scientific Research Projects Coordination for their financial support (Project Number: 2013-52) and Aksaray University, Science and Technology Application and Research Center, Turkey.

Appendix A. Supplementary Data
CCDC 1944106 contains the supplementary crystallographic data for MeNap-Pz Ligand. Copies of this information may be obtained free of charge from The Director, CCDC, 12 Union. Road, Cambridge CB2 1EZ, UK (Fax:+44-1223-336033;deposit@ccdc.cam.ac.uk or http://www.ccdc.cam.ac.uk).

Supplementary data associated with this article can be found at the end of this manuscript.

References

1. Cano M, Heras JV, Maeso M, Alvaro M, Ferfindez R et al. 3-[4-Phenoxyphenyl]pyrazole (Hpzpp) and 3-[4-butoxyphenyl]pyrazole (Upzbp) in rhodium chemistry. Crystal structures of 3-[4-phenoxyphenyl]pyrazole, $[Rh(\mu\text{-}pzpp)(COD)]_2.1/2CH_2Cl_2$ and $[Rh(\mu\text{-}pzbp)(COD)]_2$. Journal of Organometallic Chemistry 1997; 534: 159-172. doi: 10.1016/S0022-328X(96)06890-8
2. Chauhan A, Sharma PK, Kaushik N. Pyrazole: a versatile moiety. International Journal of ChemTech Research 2011; 3 (1): 11-17.
3. Hamed MA, El Gokha AA, Abdelwahed RER, Mohamed AA, El-Torgoman AM et al. Synthesis and biological evaluation of some new pyrazole derivatives. International Journal of Pharmaceutical Science and Research 2016; 1 (5): 4414-4421. doi: 10.13040/IJPSR.0975-8232.7(11).4414-21
4. Kane JL, Hirth BH, Liang B, Gourlie BB, Nahill S et al. Ureas of 5-Aminopyrazole and 2-Aminothiazole Inhibit Growth of Gram-Positive Bacteria. Bioorganic & Medicinal Chemistry Letters 2003; 13 (24): 4463–4466. doi.org/10.1016/j.bmcl.2003.09.013
5. Malhotra P, Pattan S, Nikalje A. Microwave assisted synthesis and antiinflammatory activity of 3,5-diaryl substituted–2-pyrazolines. Journal of Pharmacy and Pharmaceutical Sciences 2010; 2 (2): 21-26.
6. Addel-Aziz HA, El-Zahabi HAS, Dawood KM. Microwave-assisted synthesis and In-vitro anti-tumor activity of 1,3,4-Triaryl-5-N-arylpyrazole-carboxamides. European Journal of Medicinal Chemistry 2010; 45: 2427-2432. doi: 10.1016/j.ejmech.2010.02.026

7. Elgemeie GH, Zaghary WA, Amin KM, Nasr TM. New trends in synthesis of pyrazole nucleosides as new antimetabolites. Nucleosides, Nucleotides, and Nucleic Acid 2005; 24 (8): 1227-1247. doi: 10.1081/NCN-200067421

8. Kobayashi K, Uchiyama M, Ito H, Takahashi, H, Yoshizumi T et al. Discovery of novel arylpyrazole series as potent and selective opioid receptor-like 1 (ORL1) antagonists. Bioorganic Medicinal Chemistry Letters 2009; 19 (13): 3627-3631. doi: 10.1016/j.bmcl.2009.04.116

9. Lamberth C. Pyrazole chemistry in crop protection. Heterocycles 2007; 71 (7): 1467-1502. doi: 10.3987/REV-07-613

10. Jana A, Brandão P, Jana H, Jana AD, Mondal G et al. Synthesis, structure and catalytic promiscuity of a napthyl-pyrazole Mn(II) complex and structure-activity relationships. Journal of Coordination Chemistry 2019; 72 (16): 2636-2653. doi: 10.1080/00958972.2019.1658192

11. Weekes RJ, Hawes CS. Synthesis, coordination chemistry and photophysical properties of naphtho-fused pyrazole ligands. CrystEngComm 2019; 21: 5152-5163. doi: 10.1039/C9CE01074B.

12. Ali SA, Awad SM, Said AM, Mahgoub S, Taha H et al. Design, synthesis, molecular modelling and biological evaluation of novel 3-(2-naphthyl)-1-phenyl-1H-pyrazole derivatives as potent antioxidants and 15-Lipoxygenase inhibitors. Journal of Enzyme Inhibition and Medicinal Chemistry 2020; 35 (1): 847-863. doi: 10.1080/14756366.2020.1742116J.

13. He L, Duan L, Oiao J, Zhang D, Wang L et al. Enhanced stability of blue-green light-emitting electrochemical cells based on a cationic iridium complex with 2-(1-phenyl-1H-pyrazol-3-yl)pyridine as the ancillary ligand. Chemical Communications 2011; 47: 6467-6469. doi: 10.1039/C1CC11263E

14. Montoya V, Pons J, Solans X, Font-Bardia M, Ros J. Synthesis and characterisation of new N1-alkyl-3,5-dipyridylpyrazole derived ligands. Study of their reactivity with Pd(II) and Pt(II). Inorganica Chimica Acta 2005; 358: 2763-2769. doi: 10.1016/j.ica.2005.01.028

15. Prakash O, Kumar R, Sehrawat R. Synthesis and antibacterial activity of some new 2,3-dimethoxy-3-hydroxy-2-(1-phenyl-3-aryl-4-pyrazolyl) chromanones. European Journal of Medicinal Chemistry 2009; 44: 1763-1767. doi: 10.1016/j.ejmech.2008.03.028

16. Bouabdallah I, Touzani R, Zidane I, Ramdani A, Radi S. Synthesis of some 1-aryl-3,5-disubstituted-pyrazoles by N-arylation of 3,5-disubstituted-pyrazoles with 4-fluoro and 2-fluoronitrobenzene under microwave irradiation and classical heating. Arkivoc 2006; 12: 138-144. doi: 10.3998/ark.5550190.0007.c16

17. Monnier F, Taillefer MA. Catalytic C-C, C-N, and C-O Ullmann-type coupling reactions. Angewandte Chemie International Edition 2009; 48: 6954-6971. doi: 10.1002/anie.200804497

18. Wolf JP, Tomori H, Sadighi JP, Yin J, Buchwald SLJ. Simple, efficient catalyst system for the palladium-catalyzed amination of aryl chlorides, bromides, and triflates. Journal of Organic Chemistry 2000; 65 (4): 1158-1174. doi: 10.1021/jo991699y

19. Xu ZL, Li HX, Ren ZG, Du WY, Xu WC et al. $Cu(OAc)_2 \cdot H_2O$-catalyzed N-arylation of nitrogen-containing heterocycles. Tetrahedron 2011; 67 (29) 5282-5288. doi: 10.1016/j.tet.2011.05.025

20. Suh J, Kang HS, Kim JE, Yum EK. Diversification of pyrazoles by microwave-assisted ligand free copper catalyzed N-arylation. Bulletin Korean Chemical Society 2012; 33 (6): 2067-2070. doi: 10.5012/bkcs.2012.33.6.2067

21. Sugaya T, Mimury Y, Ikuta M, Mimury T, Kasai M et al. Synthesis of a 6H-Pyrazolo[4,5,1-de]acridin-6-one derivative: A useful intermediate of antitumour agents. Synthesis 1994; 1: 73-76. doi: 10.1055/s-1994-25408

22. Park KH, Cho SY, Kim SS, Yum EK, Yu CM et al. Novel migration of aryl group in 3-trifluoromethylpyrazolyl aryl ether. Bulletin Korean Chemical Society 1995; 16: 799-801.

23. Roy S, Roy S, Gribble GW (2012) Metalation of Pyrazoles and Indazoles. In: Gribble G (editor). Metalation of Azoles and Related Five-Membered Ring Heterocycles. Topics in Heterocyclic Chemistry, vol 29. Berlin, Heidelberg, Germany: Springer, doi: 10.1007/7081_2012_82

24. Chen R, Liu CS, Zhang H, Guo Y, Bu XH et al. Three new Cu(II) and Cd(II) complexes with 3-(2-pyridyl)pyrazole-based ligand: Syntheses, crystal structures, and evaluations for bioactivities. Journal of Inorganic Biochemistry 2007; 101: 412-421. doi: 10.1016/j.jinorgbio.2006.11.001

25. Bushuev M., Krivopalov VP, Semikolenova NV, Shvedenkov YG, Sheludyakova LA et al. Cu(II) Complexes with 4,6-Bis(3,5-dimethyl-1H-pyrazole-1-yl)pyrimidine,4-(3,5-dimethyl-1H-pyrazole-1-yl)-6-(3,5-diphenyl-1H-pyrazole-1-yl)pyrimidine: Synthesis and catalytic activity in ethylene polymerization reaction. Russian Journal of Coordination Chemistry 2007; 33: 8, 601-606. doi: 10.1080/00958972.2012.657187

26. Zhang H, Liu CS, Bu XH, Yang M. Synthesis, crystal structure, cytotoxic activity and DNA-binding properties of the copper (II) and zinc (II) complexes with 1-[3-(2-pyridyl)pyrazol-1-ylmethyl]naphthalene. Journal of Inorganic Biochemistry 2005; 99: 1119-1125. doi: 10.1016/j.jinorgbio.2005.02.005

27. Keter FK, Darkwa J. Perspective: the potential of pyrazole-based compounds in medicine. Biometals 2012; 25: 9-21. doi: 10.1007/s10534-011-9496-4

28. Molander GA, Ryu DW, Sarvari MH, Devulapally R, Seapy DG. Suzuki-Miyaura cross-coupling of potassium trifluoro(N-methylheteroaryl) borates with aryl and heteroaryl halides. Journal of Organic Chemistry 2013; 78: 6648-6656. doi: 10.1021/jo4009589

29. Boswell MG, Yeung FG, Wolf C. Copper-catalyzed C-N bond formation with N-heterocycles and aryl halides. Synlett 2012; 23 (8): 1240-1244. doi: 10.1055/s-0031-1290827

30. Wang XY, Liu SQ, Zhang CY, Song G, Bai FY et al. Synthesis, structural, and biological evaluation of the arene-linked pyrazolyl methane ligands and their d9/d10 metal complexes. Polyhedron 2012; 47: 151-164. doi: 10.1016/j.poly.2012.08.016

31. Hurtado J, Ibanez A, Rojas R, Valderrama M, Fröhlich R. Organonickel(II) comlexes with anionic tridentate 1,3-bis(azolylmethyl)phenyl ligands. Synthesis, structural chracterization and catalytic behavior. Journal of Brazilian Chemical Society 2011; 22: 1750-1757. doi: 10.1590/S0103-50532011000900018

32. SADABS, Version 6.02; Bruker Inc.: Madison, WI, 1998-2000.

33. SHELXTL, Version 6.10; Bruker Inc.: Madison, WI, 1998-2000.

34. Farrugia LJ. ORTEP-3 for Windows-a version of ORTEP-III with a Graphical User Interface (GUI) J. Appl. Crystallogr 1997; 30: 565. doi: 10.1107/S0021889897003117

35. Jorgensen, JH, Turnidge JD. Susceptibility test methods: dilution and disk diffusion methods, In: Jorgensen JH, Pfaller MA, Carroll KC, Funke G, Landry ML et al. (editors). Manual of Clinical Microbiology. 11th ed. American Society for Microbiology Press, Washington, USA, 2015; 71: 1253-1273. doi: 10.1128/9781555817381.ch71

36. Mahesh B, Satish S. Antimicrobial activity of some important medicinal plant against plant and human pathogens. World Journal of Agricultural Sciences 2008; 4 (5): 839-843.

37. Wayne, P. National committee for clinical laboratory standards. Performance standards for antimicrobial disc susceptibility testing, Wayne, USA, 2002; 12.

38. Wang DJ, Zheng CY, Fan L. Synthesis, characterization, and crystal structures of new 3,5-diaryl-1H-pyrazoles. Journal of Molecular Structure 2009; 938: 311-315. doi: 10.1016/j.molstruc.2009.10.001

39. Nakamato K. Infrared and Raman Spectra of Inorganic and Coordination Compounds, Part B: Applications in Coordination, Organometallic, and Bioinorganic Chemistry. 6th ed. New Jersey, USA: John Wiley & Sons, Inc., 2009. doi: 10.1002/9780470405888

40. Curtis NF, Curtis YM. Some nitrato-amine nickel(II) compounds with monodentate and bidentate nitrate ions. Inorganic Chemistry 1965; 4: 804-809. doi: 10.1021/ic50028a007

41. Potapov AS, Khlebnikov AI. Synthesis of mixed-ligand copper(II) complexes containing bis(pyrazol-1-yl)methane ligands. Polyhedron 2006; 25: 2683-2690. doi: 10.1016/j.poly.2006.03.016

42. Bagihalli GB, Avaji PG, Patil SA, Badami PS. Synthesis, spectral characterization, in vitro antibacterial, antifungal and cytotoxic activities of Co(II), Ni(II) and Cu(II) complexes with 1,2,4-triazole Schiff bases. European Journal of Medicinal Chemistry 2008; 43: 2639-2649. doi: 10.1016/j.ejmech.2008.02.013

43. Skoog DA, Holler FJ, Nieman TA. Principles of Instrumental Analysis. 5th ed. Florida, USA: Harcourt Brace &Company, 1998.

44. Balcı M. Nükleer Manyetik Rezonans Spektroskopisi, İkinci Basım, ODTÜ Yayıncılık, Ankara, 2004 (in Turkish).

45. Yang G, Raptis RG. Synthesis, characterization and crystal structures of two 2-naphthyl substituted pyrazoles. Journal of Heterocyclic Chemistry 2003; 40: 659-664. doi: 10.1002/jhet.5570400416

46. Sharma S, Barooah N, Baruah JB. Tris (3,5-dimethylpyrazole) copper(II) nitrate: as an oxidation catalyst. Journal of Molecular Catalysis A: Chemical 2005; 229: 171-176. doi: 10.1016/j.molcata.2004.11.019

47. Geary WJ. The Use of conductivity measurements in organic solvents for the characterization of coordination compounds. Coord. Chem. Rev 1971; 7: 81-122. doi: 10.1016/S0010-8545(00)80009-0

48. Sunitha S. Synthesis and characterization of biologically important metal complexes. PhD, University of Calicut, Kerala, India, 2008.

49. Wu F, Tong H, Wang K, Zhang X, Zhang J et al. Mononuclear copper(I) bromide complexes chelated with bis(pyrazol-1-ylmethyl)-pyridine ligands: Structures, electronic properties and solid state photoluminescence. Journal of Luminescence 2016; 177: 82-87. doi: 10.1016/j.jlumin.2016.04.021

50. Hathaway BJ, Billing DE. The electronic properties and stereochemistry of mono-nuclear complexes of the copper(II) ion. Coordination Chemistry Reviews 1969; 5: 143-207. doi: 10.1016/S0010-8545(00)80135-6

51. Reddy SL, Endo T, Reddy GS. Electronic (Absorption) Spectra of 3D transition metal complexes, advanced aspects of spectroscopy. IntechOpen 2012; 548. doi: 10.5772/50128

52. Ray RK, Kauffman GB. EPR spectra and covalency of bis(amidinourea/o alkyl-1-amidinourea)copper(II) complexes, Part II. Properties of the CuN_4^{2-} chromophore. Inorganica Chimica Acta 1990; I73: 207-214. doi: 10.1016/S0020-1693(00)80215-7

53. Shanmugakala R, Tharmaraj P, Sheela CD. Synthesis and spectral studies on metal complexes of s-triazine based ligand and non linear optical properties. Journal of Molecular Structure 2014; 1076: 606-613. doi: 10.1016/j.molstruc.2014.08.012

54. Benial AMF, Ramakrishnan V, Murugesan R. Single crystal EPR of $Cu(C_5H_5NO)_6(BF_4)_2$: an example of admixed ground state. Spectrochimica Acta Part A 2000; 56: 2775-2781. doi: 10.1016/S1386-1425(00)00322-X

Supplement

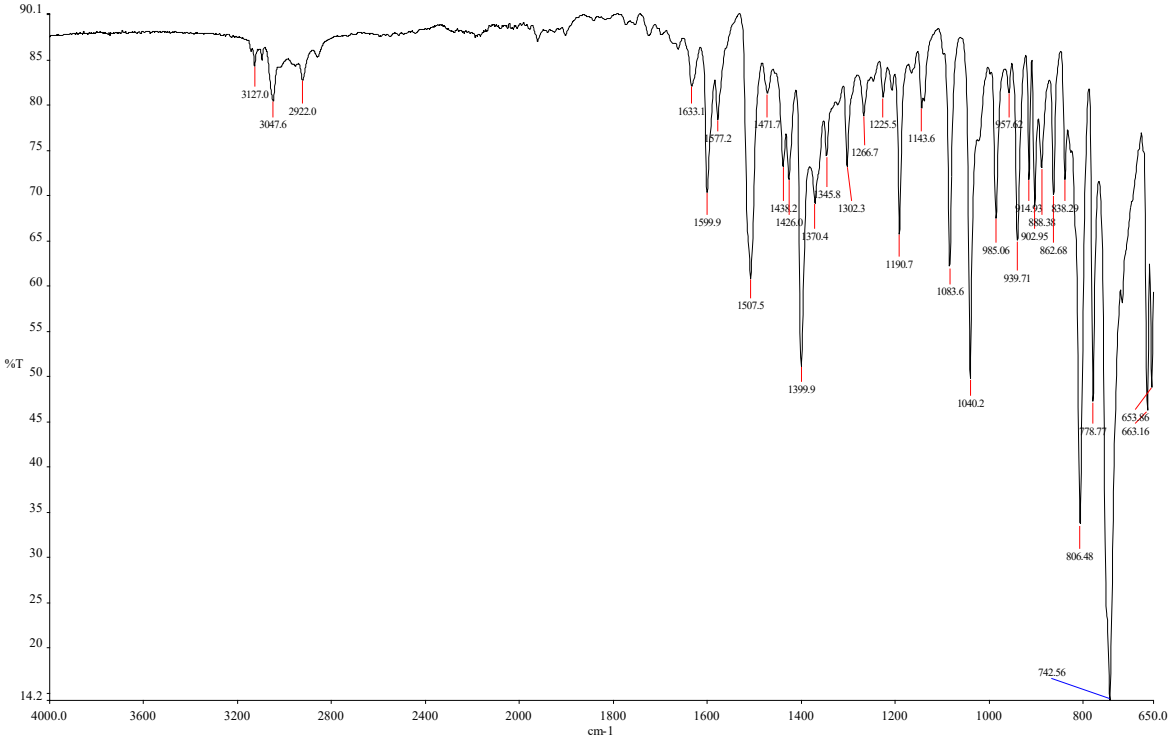

Figure S1. FT-IR spectrum of MeNap-Pz ligand.

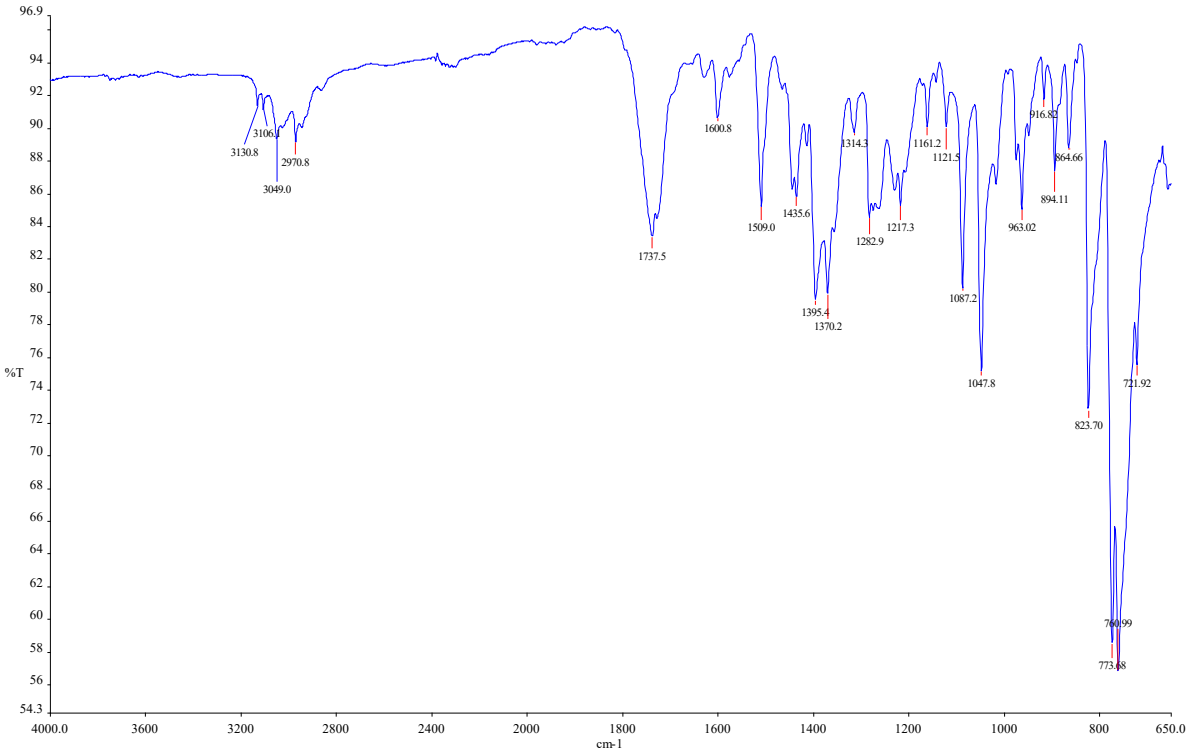

Figure S2. FT-IR spectrum of NapMe-Pz ligand.

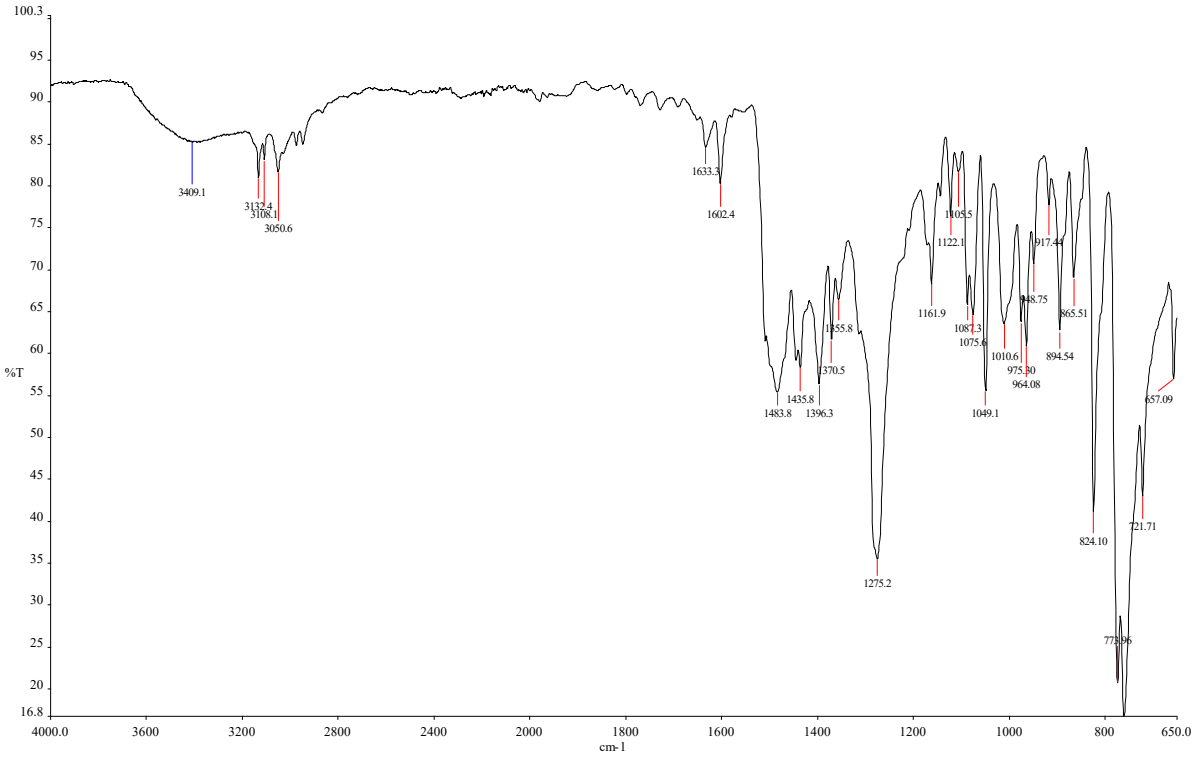

Figure S3. FT-IR spectrum of $[Cu(NapMe\text{-}Pz)_2(NO_3)_2].H_2O$ complex.

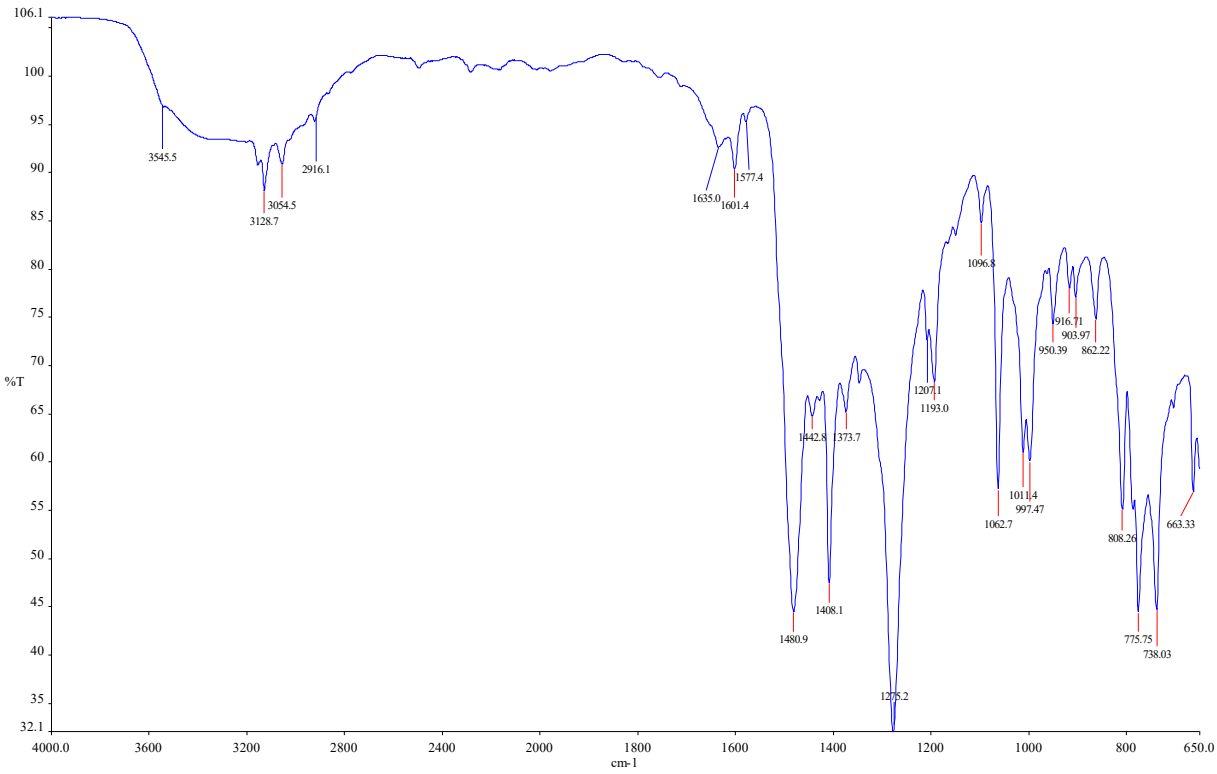

Figure S4. FT-IR spectrum of $[Cu(MeNap\text{-}Pz)_2(NO_3)]NO_3.2H_2O$ complex.

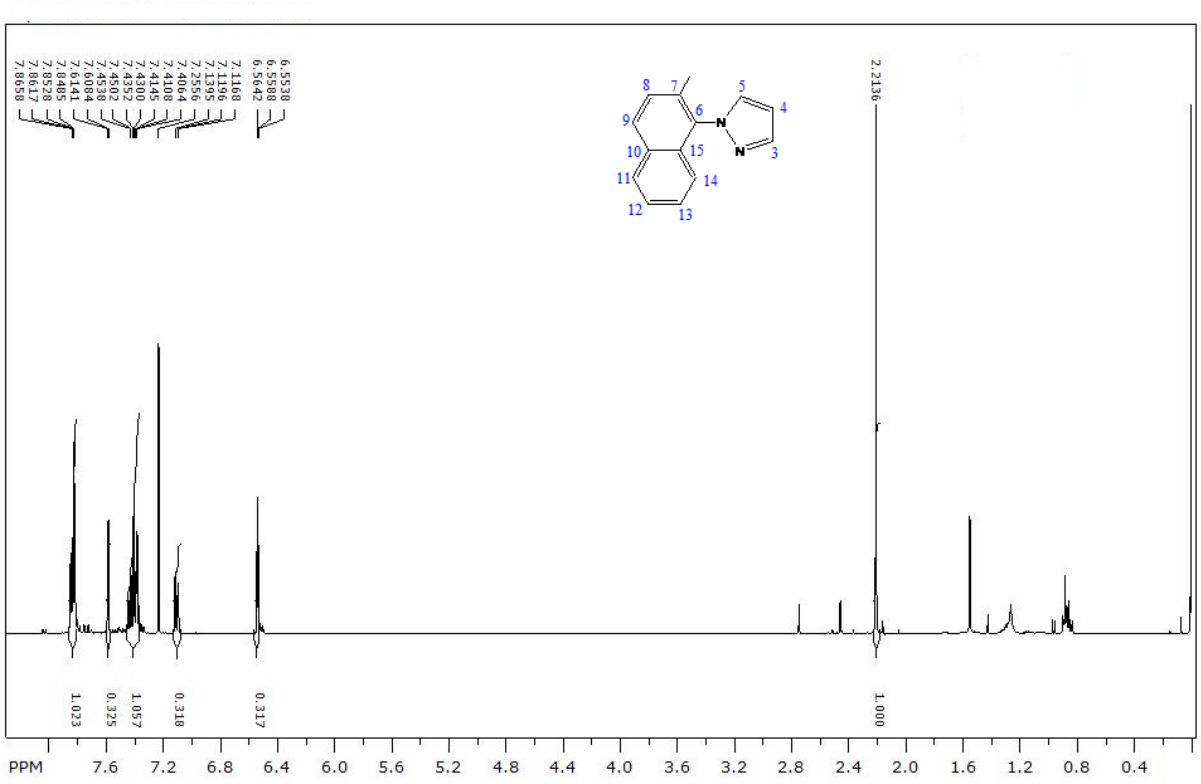

Figure S5. ^{1}H-NMR spectrum of MeNap-Pz ligand recorded in $CDCl_3$ and 400 MHz.

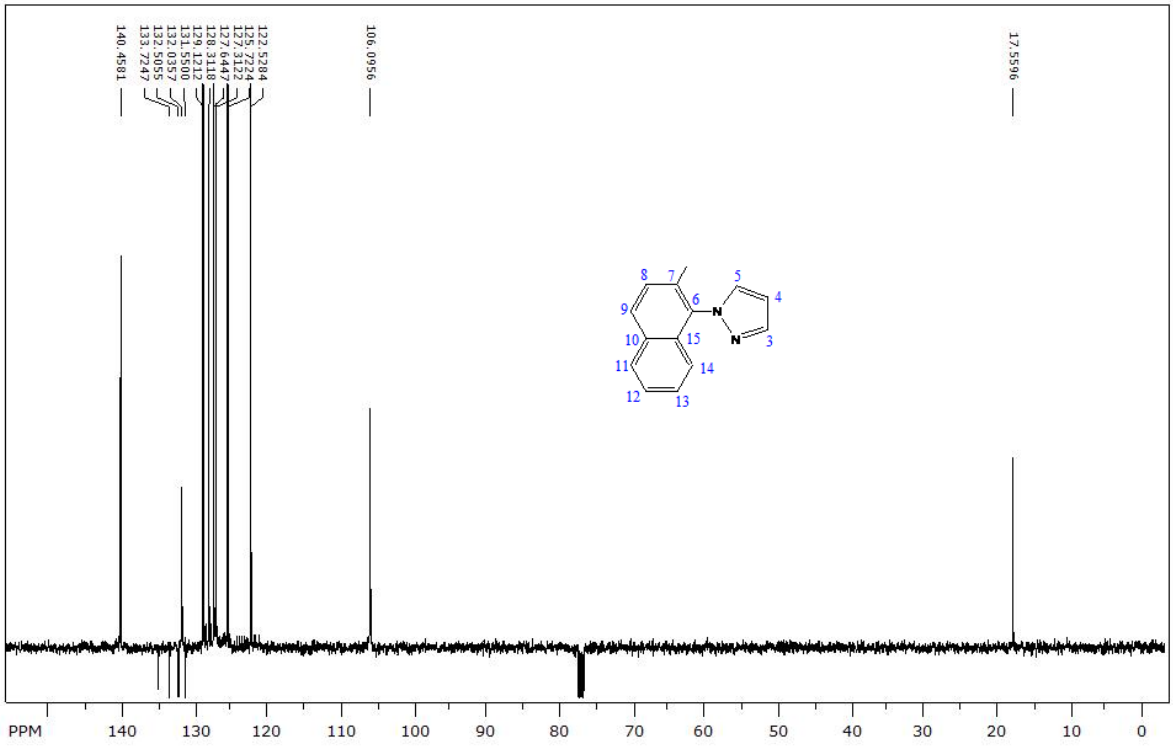

Figure S6. ^{13}C-NMR (ATP) spectrum of MeNap-Pz ligand recorded in $CDCl_3$ and 100.6 MHz.

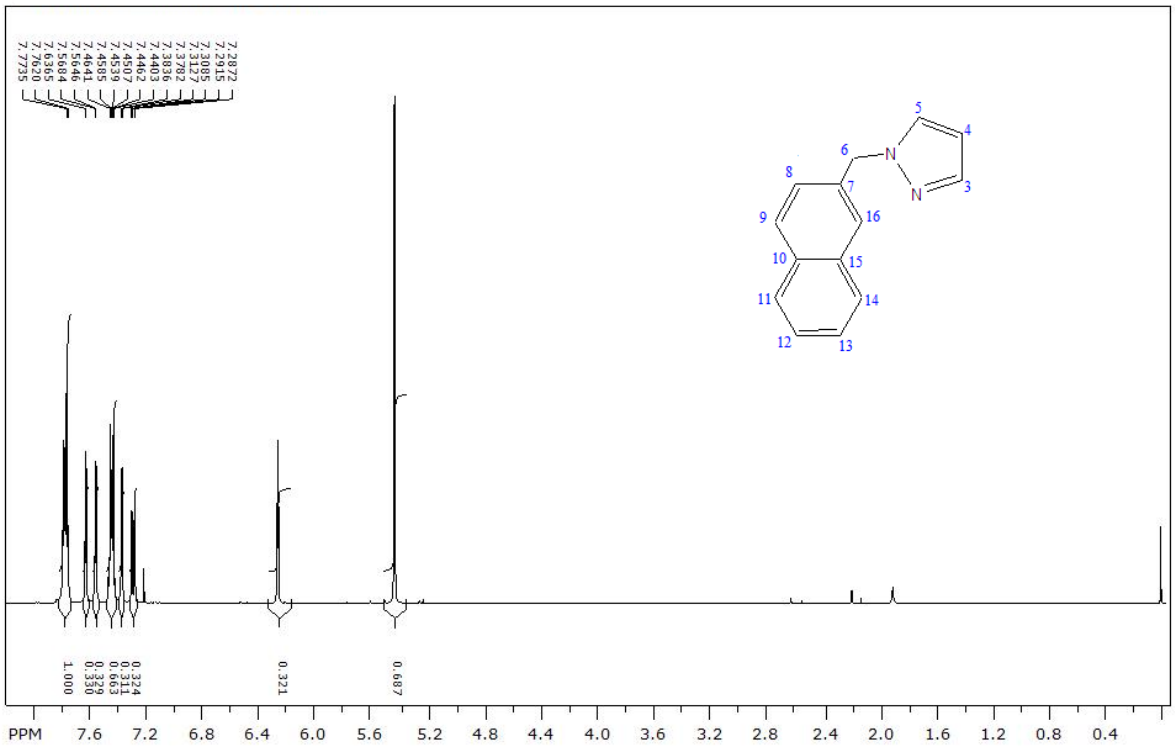

Figure S7. ^{1}H-NMR spectrum of NapMe-Pz ligand recorded in $CDCl_3$ and 400 MHz.

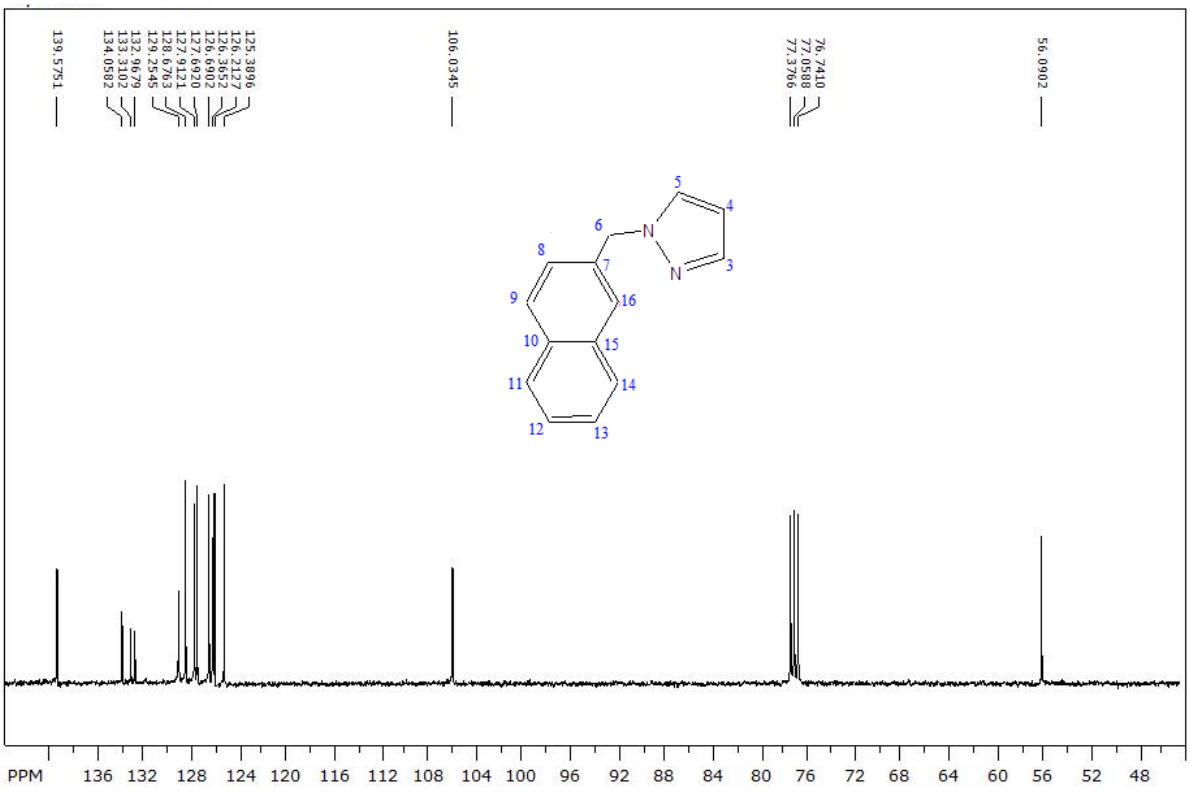

Figure S8. ^{13}C-NMR spectrum of NapMe-Pz ligand recorded in $CDCl_3$ and 100.6 MHz.

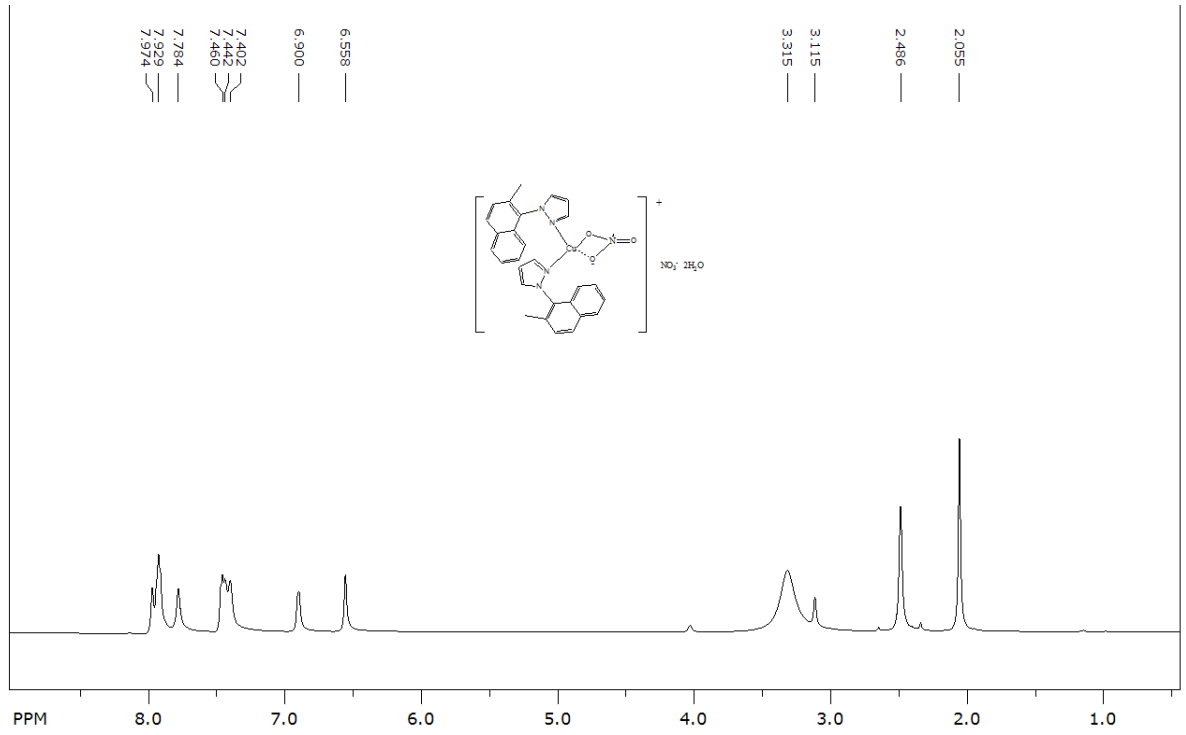

Figure S9. ^{1}H-NMR spectrum of $[Cu(MeNap\text{-}Pz)_2(NO_3)]NO_3.2H_2O$ complex recorded in DMSO-d_6 and 600 MHz.

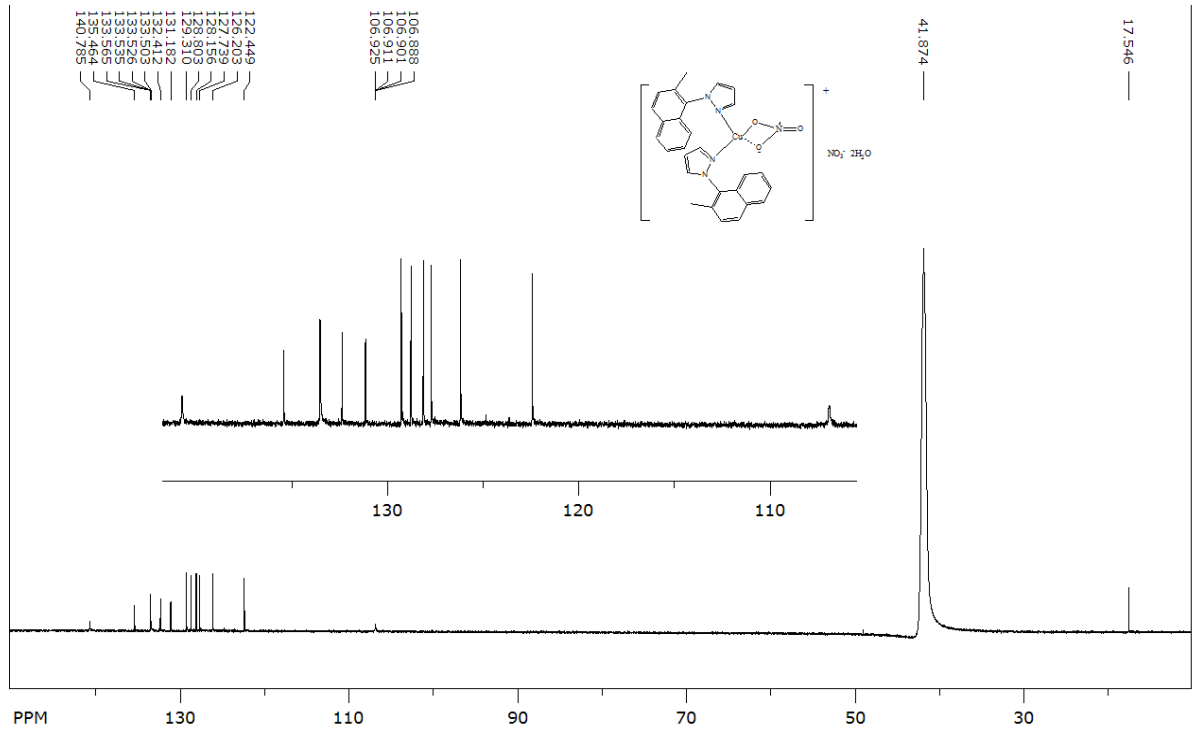

Figure S10. ^{13}C-NMR spectrum of $[Cu(MeNap\text{-}Pz)_2(NO_3)]NO_3.2H_2O$ complex recorded in DMSO-d_6 and 150 MHz.

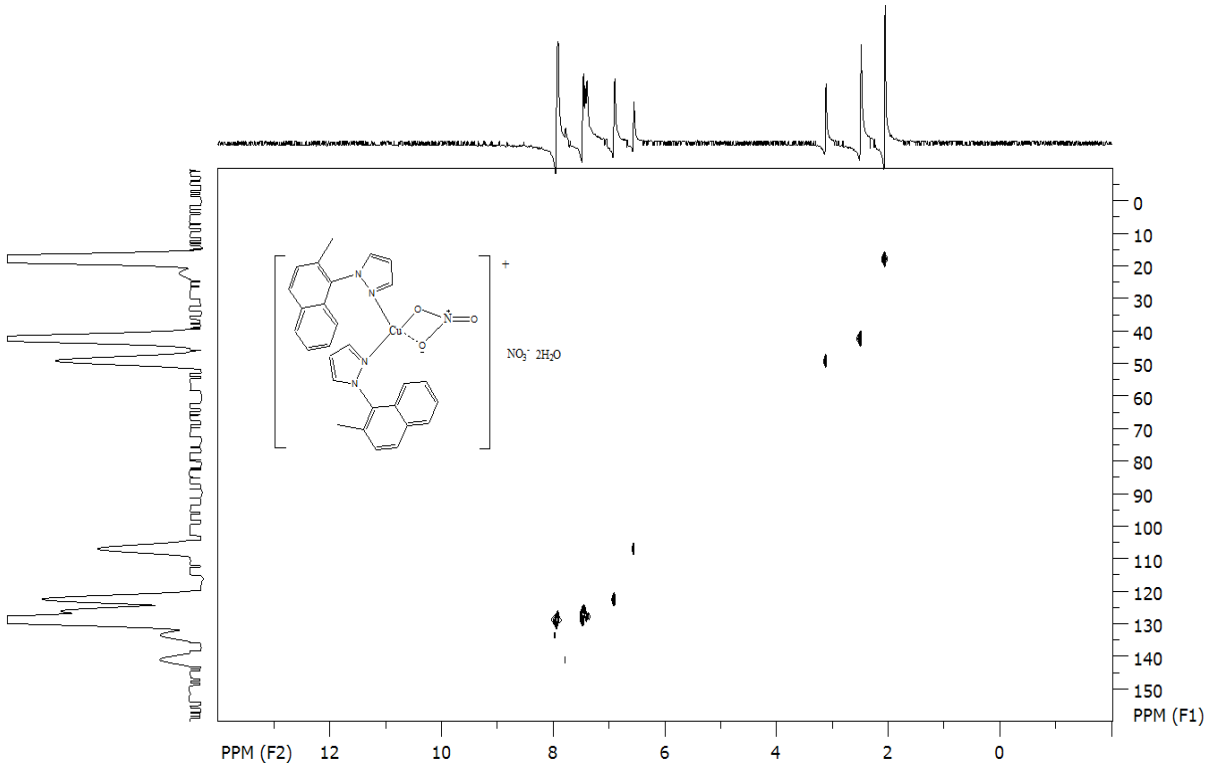

Figure S11. HETCOR-NMR spectrum of $[Cu(MeNap\text{-}Pz)_2(NO_3)]NO_3.2H_2O$ complex.

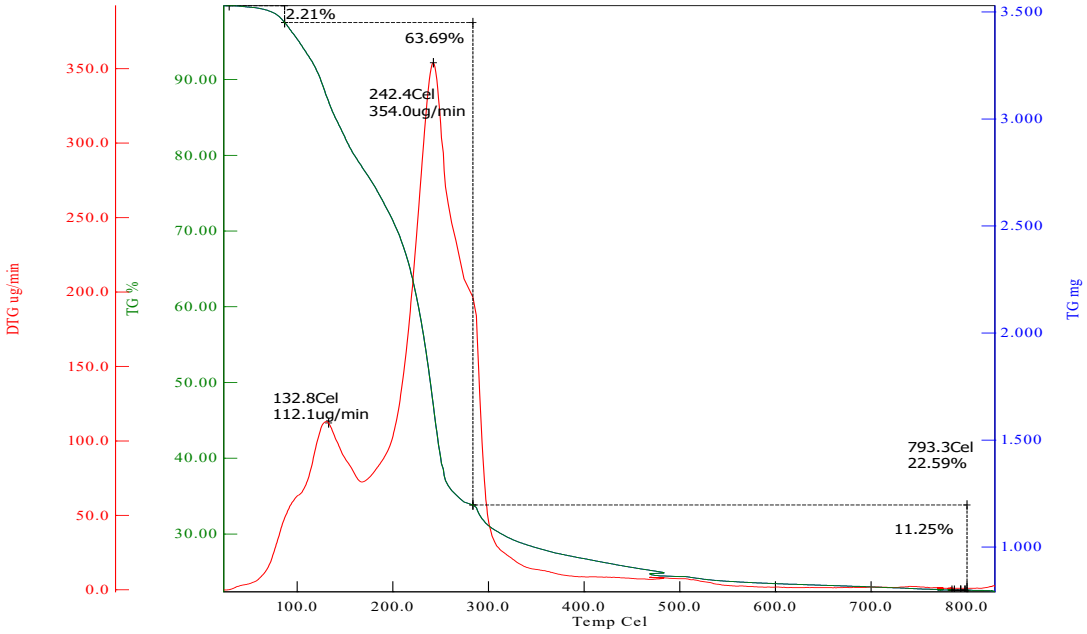

Figure S12. TG-DTG curves of $[Cu(NapMe\text{-}Pz)_2(NO_3)_2].H_2O$ complex.

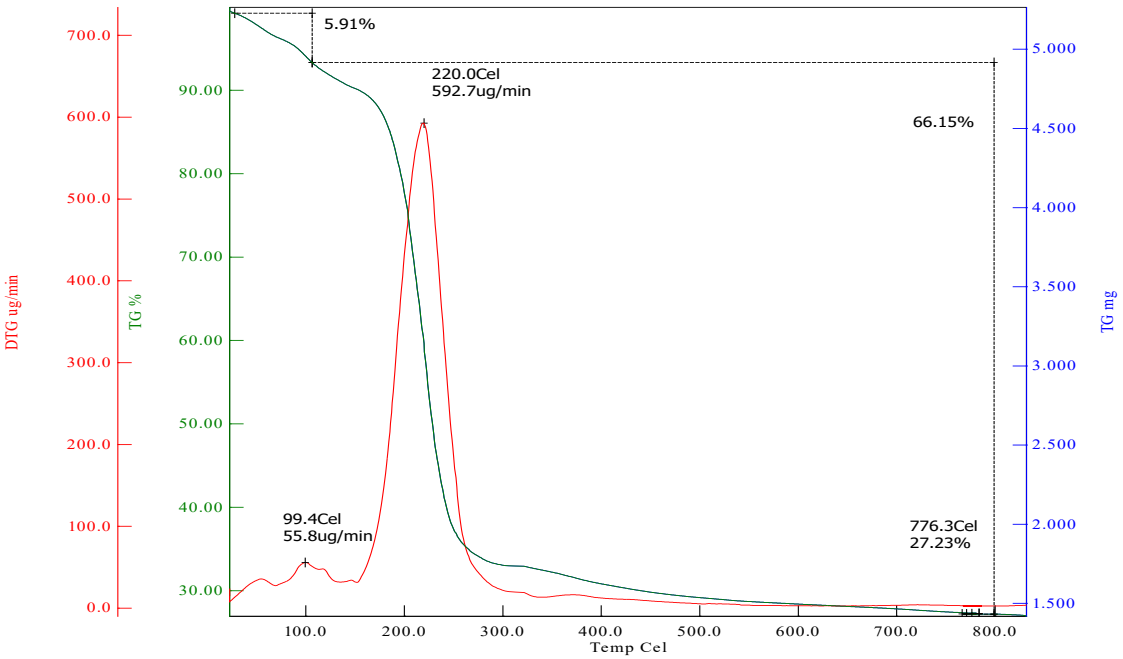

Figure S13. TG-DTG curves of $[Cu(MeNap\text{-}Pz)_2(NO_3)]NO_3.2H_2O$ complex.

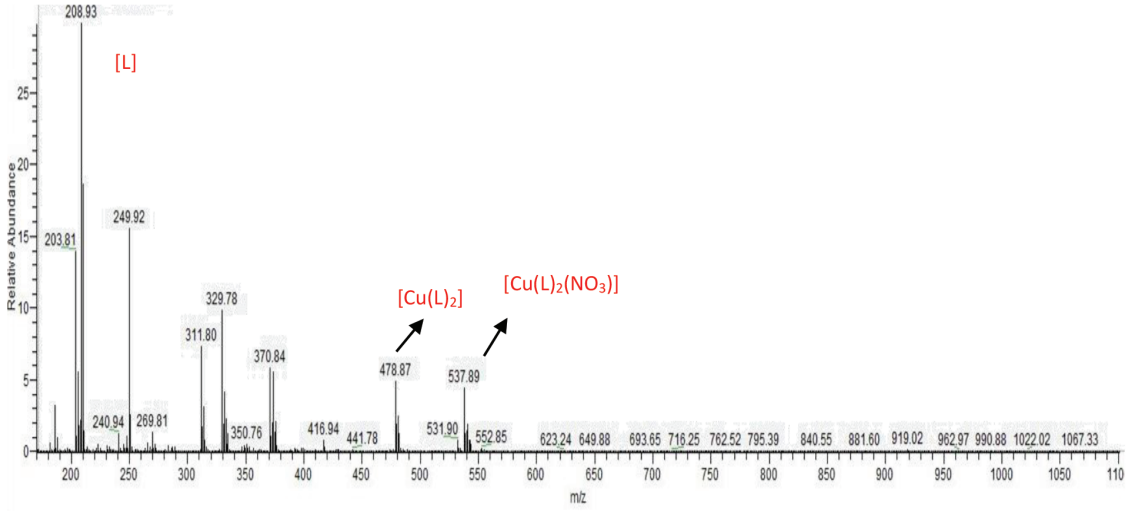

Figure S14. Mass spectrum of MeNap-Pz ligand.

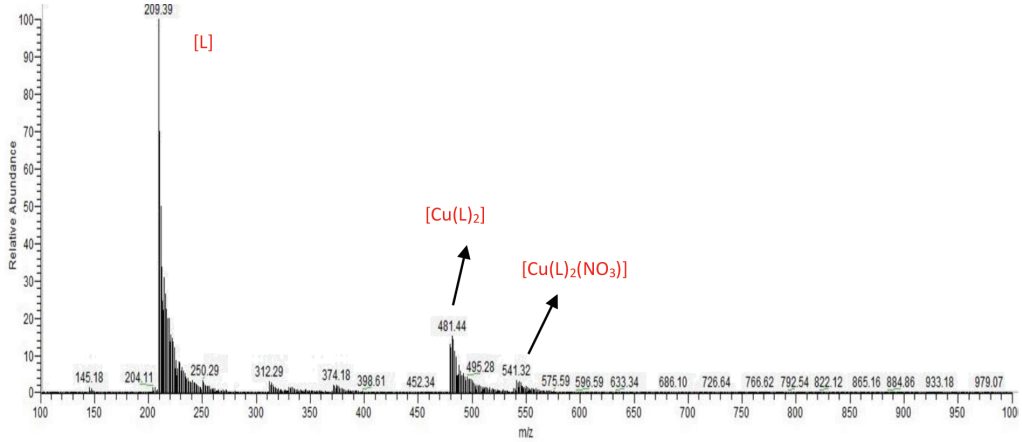

Figure S15. Mass spectrum of NapMe-Pz ligand.

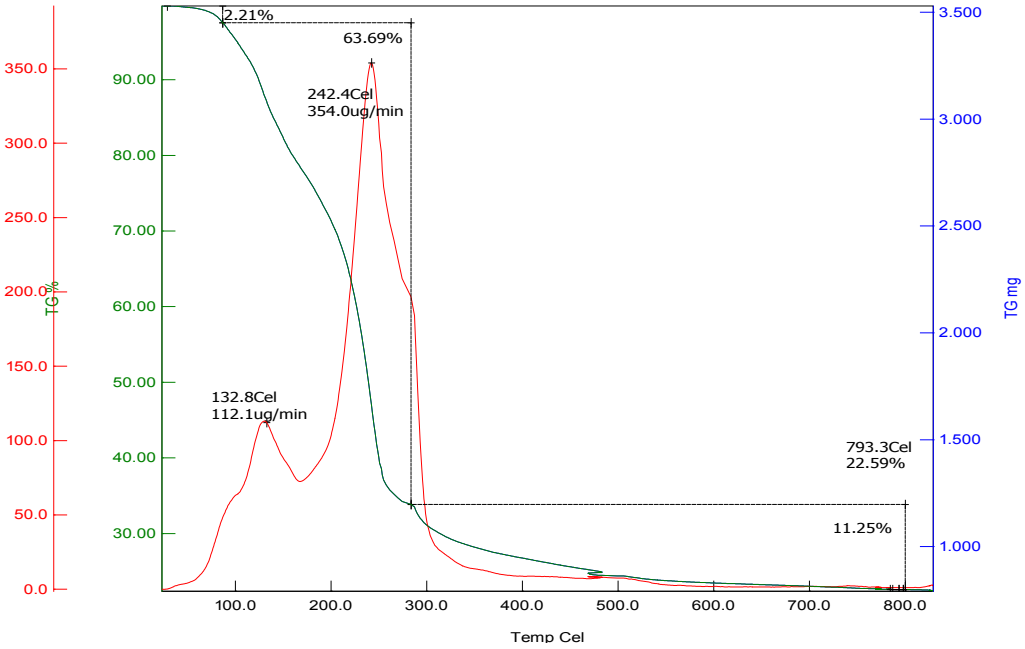

Figure S16. Mass spectrum of $[Cu(NapMe\text{-}Pz)_2(NO_3)_2].H_2O$ complex.

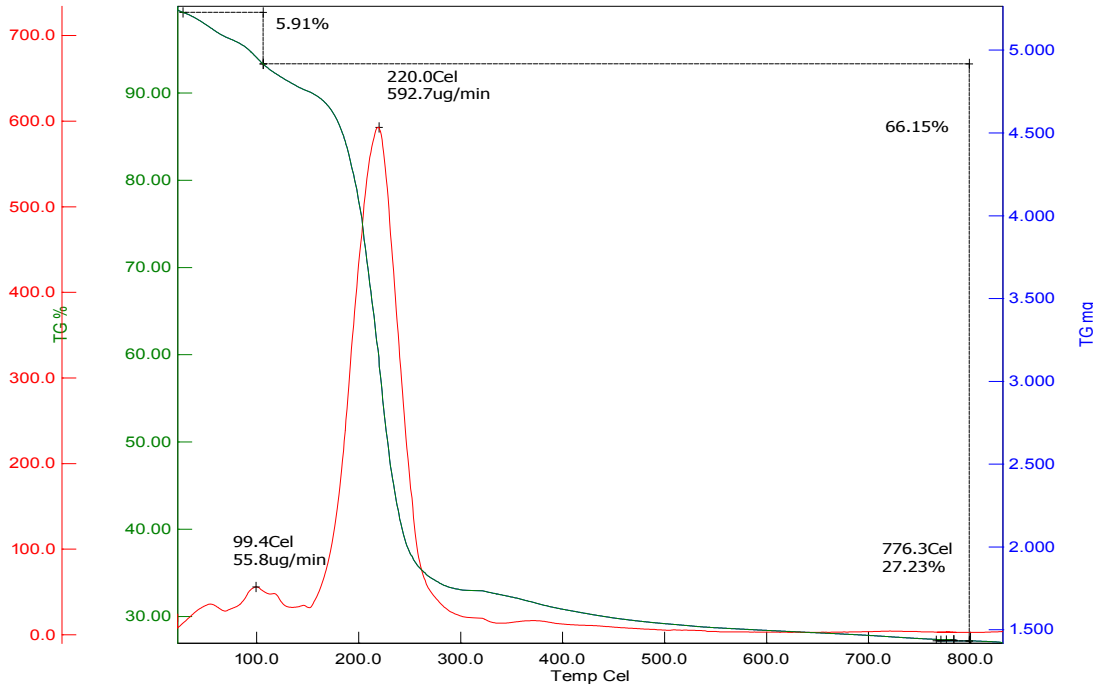

Figure S17. Mass spectrum of $[Cu(MeNap\text{-}Pz)_2(NO_3)]NO_3.2H_2O$ complex.

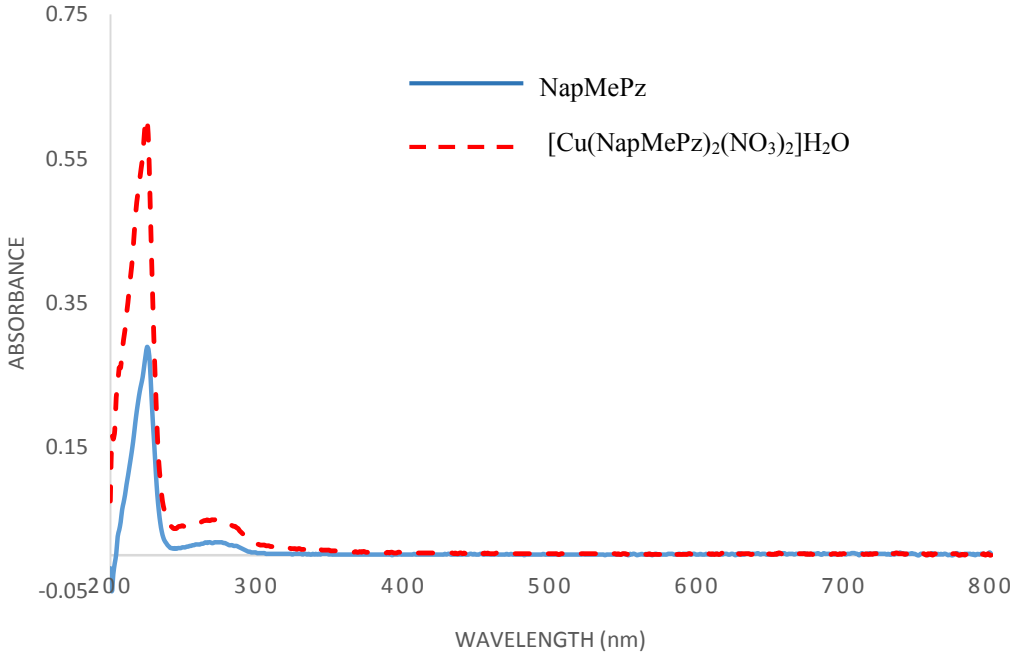

Figure S18. UV-Vis spectrum of NapMe-Pz ligand and its Cu(II) complex.

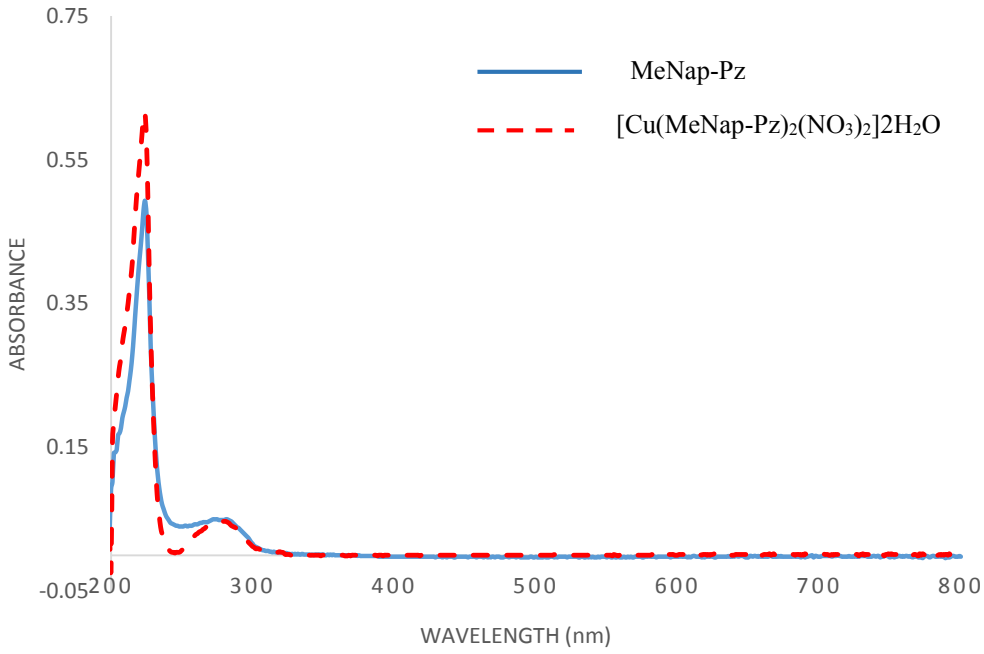

Figure S19. UV-Vis spectrum of MeNap-Pz ligand and its Cu(II) complex.

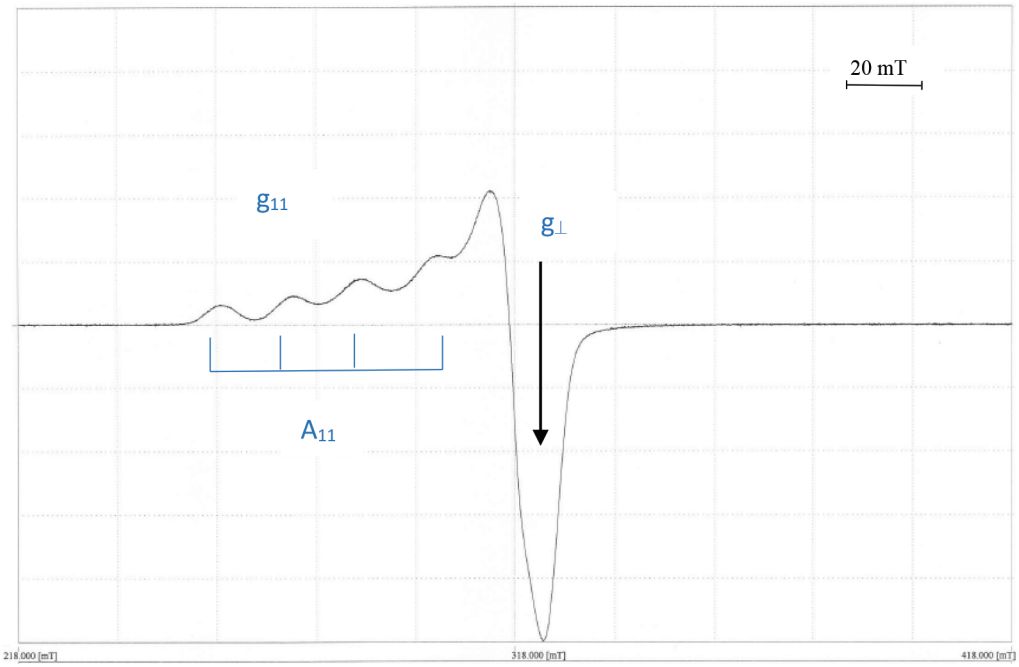

Figure S20. ESR spectrum of $[Cu(NapMe\text{-}Pz)_2(NO_3)_2].H_2O$ complex.

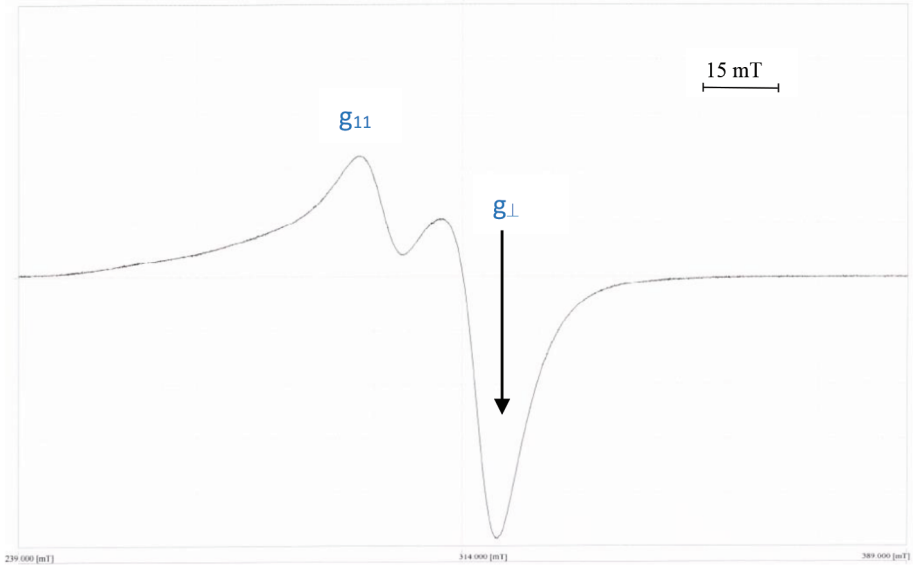

Figure S21. ESR spectrum of $[Cu(MeNap\text{-}Pz)_2(NO_3)]NO_3.2H_2O$ complex.

Table S1. UV-Vis spectra of ligands and their metal complexes.

Compounds	$\lambda_{max.}$ (nm)	ε ($M^{-1}cm^{-1}$)	Transitions
NapMe-Pz	225 273	97306 6060	n-π^* $\pi-\pi^*$
$[Cu(NapMe\text{-}Pz)_2(NO_3)_2].H_2O$	225 274	157198 13229	n-π^* $\pi-\pi^*$
MeNap-Pz	224 281	10000 1010	n-π^* $\pi-\pi^*$
$[Cu(MeNap\text{-}Pz)_2(NO_3)]NO_3.2H_2O$	223 279	130851 10000	n-π^* $\pi-\pi^*$

Table S2. ESR parameters for Cu(II) complexes.

Complex	g_{11}	$g_{\perp}$	A_{11} x10^{-4} cm^{-1}	$A_{\perp} \times 10^{-4}$ cm^{-1}	G
$[Cu(MeNap\text{-}Pz)_2(NO_3)]NO_3.2H_2O$	2.21	2.05	---	---	3.9
$[Cu(NapMe\text{-}Pz)_2(NO_3)_2].H_2O$	2.35	2.03	157	99	10.6